From Department of Medical Biochemistry and Biophysics
Karolinska Institutet, Stockholm, Sweden

SPATIAL REGULATION OF MEMBRANE RECEPTOR SIGNALING USING DNA ORIGAMI

Trixy Fang

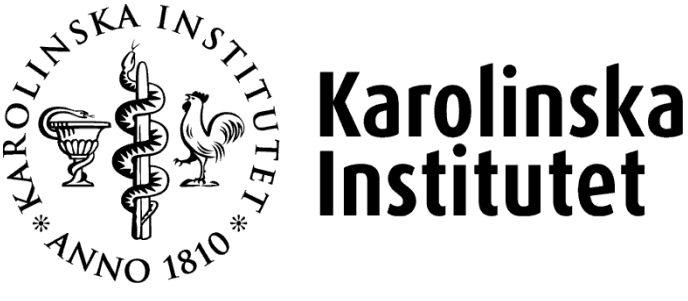

Stockholm 2021

Published by Karolinska Institutet.
Printed by Universitetsservice US-AB, 2021

ISBN 978-91-8016-150-3
On the cover: Stylized rendering of DNA origami nanostructures presenting protein patterns to cell membrane proteins.

Spatial regulation of membrane receptor signaling using DNA origami

THESIS FOR DOCTORAL DEGREE (Ph.D.)

By

Trixy Fang

The thesis will be defended in public at Lecture Hall Nils Ringertz (D0351), Biomedicum, Solnavägen 9, on **6 May 2021**, **9:30**.

Principal Supervisor:
Ana Teixeira, PhD, Docent
Karolinska Institutet
Department of Medical Biochemistry and Biophysics
Division of Biomaterials

Co-supervisor(s):
Professor Björn Högberg
Karolinska Institutet
Department of Medical Biochemistry and Biophysics
Division of Biomaterials

Opponent:
Assistant Professor Erdinc Sezgin
Karolinska Institutet
Department of Women's and Children's Health

Examination Board:
Lisa Westerberg, PhD, Docent
Karolinska Institutet
Department of Microbiology, Tumor and Cell Biology

Professor Michael Malkoch
KTH Royal Institute of Technology
Department of Fibre and Polymer Technology
Division of Coating Technology

Gonçalo Castelo-Branco, PhD, Docent
Karolinska Institutet
Department of Medical Biochemistry and Biophysics
Division of Molecular Neurobiology

“But in the end, it’s only a passing thing...this shadow.

Even darkness must pass.”

— J.R.R Tolkien, The Lord of the Rings

POPULAR SCIENCE SUMMARY OF THE THESIS

Individual cells within multicellular organisms must communicate with each other in order to ensure the proper function of the organism as a whole. Cell communication can be of many forms and one of which is by direct contact between interacting cells. Much like using the sense of touch as a form of language, cells use proteins on their surface to sense other interacting cells. It has been hypothesized that cells communicate with each other through their cell surface proteins and react differently depending on the distances and patterns these proteins are placed on. These distances are at the nanoscale and it is very difficult to build protein patterns at such a small scale and with precision. A way to achieve this is to use DNA molecules to build structures that allow attaching of proteins at the nanoscale. In this thesis, we use this method to make very precise patterns of proteins and find out how cells respond to different protein patterns.

ABSTRACT

Juxtracrine signaling between apposing membrane receptors and ligands is an important class of intercellular communication. Much focus has been directed towards studying the biochemical interactions between receptors and ligands, their surface expression levels and signaling activities for driving downstream signaling processes. However, the lateral distribution of receptors/ligands on the membrane has been gaining increasing significance in modulating intercellular signaling. Nevertheless, little is known about the cellular mechanisms of interpreting this biophysical factor during ligand/receptor signaling. The work in thesis is based on the hypothesis that cells use information from the spatial organization of their surface ligands/receptors to direct intracellular signaling. To address this, we have employed the power of DNA origami technology to manipulate ligand spatial distances with nanometer precision and constrain their cognate receptors into defined configurations in ephrin/Eph signaling and the T-cell negative regulators PD-L1/PD-1 on T cell signaling. With this approach, we demonstrated that modulating the nanoscale organization of ephrin-A5 ligands contributed to divergent transcriptional profiles in human glioblastoma cells (paper I). We also showed that the nanoscale organization of PD-L1 regulates T-cell activation and sizes of PD-1 clusters (paper II). In summary, this work describes that the spatial organization of ligands/receptors at the nanoscale can serve as an important physical guidance cue that tunes the overall cellular response.

LIST OF SCIENTIFIC PAPERS

I. Toon Verheyen*, **Trixy Fang***, Dominik Lindenhofer, Yang Wang, Karen Akopyan, Arne Lindqvist, Björn Högberg, Ana I Teixeira. Spatial organization-dependent EphA2 transcriptional responses revealed by ligand nanocalipers. *Nucleic Acids Res*. 2020 Jun 4;48(10):5777-5787.

II. **Trixy Fang**, Jonatan Alvelid, Joel Spratt, Elena Ambrosetti, Ilaria Testa, Ana I Teixeira. Spatial regulation of T-cell signaling by Programmed Death-Ligand 1 on wireframe DNA origami. *ACS Nano*. 2021 Feb 23;15(2):3441-3452.

*These authors contributed equally.

CONTENTS

LIST OF ABBREVIATIONS

ADAM	A disintegrin and metalloprotease domain-containing protein
AFM	Atomic force microscopy
AP1	Activator protein 1
APC	Antigen-presenting cell
BSA	Bovine serum albumin
CD	Cluster of differentiation
cDNA	Complementary DNA
CRK	Chicken tumor virus number 10 regulator of kinase
cSMAC	Central supramolecular activation cluster
DBCO	Dibenzocyclooctyne
DE	Differentially expressed
DNA	Deoxyribonucleic acid
dSMAC	Distal supramolecular activation cluster
EGF	Epidermal growth factor
ELISA	Enzyme-linked immunosorbent assay
Eph	Erythropoietin-producing hepatoma
ERK	Extracellular signal-regulated kinases
GBM	Glioblastoma multiforme
GPI	Glycosylphosphatidylinositol
GTP	Guanine triphosphate
HEK	Human embryonic kidney
His_6	6-histidine
ICAM-1	Intercellular adhesion molecule 1
IL-2	Interleukin-2
ITAM	Immunoreceptor tyrosine activation motif

ITIM	Immunoreceptor tyrosine-based inhibitory motif
ITSM	Immunoreceptor tyrosine-based switch motif
LAT	Linker of activated T cells
LCK	Lymphocyte-specific protein tyrosine kinase
LFA-1	Lymphocyte function-associated antigen 1
MAPK	Mitogen-activated protein kinases
MHC	Major histocompatibility complex
MOI	Multiplicity of infection
MSCV	Murine stem cell retrovirus
NCK	Non-catalytic region of tyrosine kinase
NF-κB	Nuclear factor-κB
NFAT	Nuclear factor of activated T cells
NHS	*N*-hydroxysuccinimide
PAGE	Polyacrylamide gel electrophoresis
PALM	Photoactivatable localization microscopy
PBS	Phosphate-buffered saline
PD-1	Programmed Death 1
PD-L1/L2	Programmed Death Ligand 1/2
PEG	Polyethylene glycol
PI3K	Phosphoinositide 3-kinase
PLA	Proximity ligation assay
pMHC	Peptide-major histocompatibility complex
pSMAC	Peripheral supramolecular activation cluster
pY	Phosphorylated tyrosine
RCA	Rolling circle amplification
Rho	Ras homology
RNA	Ribonucleic acid

RTK	Receptor tyrosine kinases
SDS	Sodium dodecyl sulfate
SHP2	Src homology 2 domain-containing tyrosine phosphatase 2
SLP-76	SH2 domain-containing leukocyte protein of 76 kDa
SMAC	Supramolecular activation cluster
SNAP	O_6-alkylguanine-DNA alkyltransferase
STED	Stimulated emission depletion
STORM	Stochastic optical reconstruction microscopy
TAE	Tris-acetate-ethylenediaminetetraacetic acid
TCR	T-cell receptor
TEM	Transmission electron microscopy
TIRFM	Total internal reflection fluorescence microscopy
ZAP-70	zeta-chain-associated protein kinase 70

1 LITERATURE REVIEW

1.1 SPATIAL ORGANIZATION OF CELL MEMBRANE PROTEINS

Cell communication is mediated by several cues that are broadly categorized as autocrine, paracrine, endocrine and juxtacrine signals. Juxtacrine cell signaling is based on direct contact of interacting cells. The recognition and binding of cell surface receptors to their cognate ligands on juxtaposed cells is translated into intracellular signals that mediate cell behavior (e.g change in gene expression). An intrinsic feature of juxtacrine signaling is the assembly of cell surface proteins into multimolecular complexes on the membrane. In particular, the physical location of membrane proteins and their organization at cell-cell junctions have emerged as a pivotal mediator in signal transduction[1–3]. The coordinated assembly of membrane-associated proteins into organized patterns is crucial for localization, enrichment, amplification or depletion of downstream signals over the course of cell signaling[1]. Erythropoietin-producing hepatoma (Eph) signaling and the T-cell immunological synapse are examples that exemplify the integral role of spatial organization within cellular interfaces for modulating signal transduction.

1.2 EPHS AND EPHRINS

Receptor tyrosine kinases (RTK) are a major type of enzyme-linked membrane receptors which regulate core cellular and developmental processes such as cell proliferation, differentiation and migration[4]. Eph receptors are the largest subfamily of RTK, consisting of nine EphA (EphA1 – A8 and A10) and four EphB receptor classes (EphB1 – B4 and B6) in humans[5]. Ephrins and Ephs have widespread roles in developmental and physiological processes including axon guidance, tissue patterning and segregation, angiogenesis, cell migration, adhesion and repulsion[6]. The EphA1 receptor was first cloned in human hepatocellular carcinoma in 1987 and then later identified as an oncogene[7,8]. In contrast to other RTK ligands which are generally soluble, Eph signaling is typically activated by Eph receptor-interacting (ephrin) proteins tethered to the cell membrane by a glycosylphosphatidylinositol (GPI) anchor (type A) or a transmembrane domain (type B) in a juxtacrine manner[5]. While EphA and EphB receptors generally bind to ephrins-A and B respectively, cross-interactions between classes of EphA and ephrin-B, or EphB and ephrin-A have been identified[9,10]. Unlike classical RTK signaling, Ephs and ephrins have dual receptor and ligand roles which can elicit bidirectional signaling in cells interacting in *trans*[6]. This phenomenon is described by signaling cascades that occur in the Eph-expressing cell (“forward signaling”) and the ephrin-expressing cell (“reverse signaling”). Forward signaling mainly involves Eph kinase-dependent activity while

reverse signaling is based on ephrin recruitment of Src family kinases[11]. Further, the complexity of ephrin-Eph signaling is demonstrated by evidence of Ephs and ephrins interacting in *cis* on the same cell surface leading to inhibition of Eph forward signaling[12–14]. Moreover, ligand and kinase-independent signaling have been discovered for certain Eph receptors[15–17], exemplifying the versatility of Eph signaling. However, this thesis focuses on Eph forward signaling.

1.2.1 Mechanistic concepts of Eph activation

Formation of higher-order ephrin/Eph clusters on the cell membrane is essential for robust Eph signal propagation[18]. Early *in vitro* studies found that potent Eph activation was induced by ephrin ligands expressed on the cell membrane and soluble oligomers from antibody pre-clustering of ephrins fused to antibody Fc fragment[18–20]. For certain Eph receptors like EphA2, the soluble ephrin-Fc dimers are able to cause receptor clustering and activation[21,22]. However, while Eph activation (typically indicated by receptor tyrosine phosphorylation) is induced by ephrin dimers and tetramers/oligomers, it is the tetramers/oligomers that result in functional cellular responses[18]. On the contrary, soluble ephrin monomers act as antagonists by binding to Eph receptors but do not elicit receptor tyrosine phosphorylation[19]. Contradictory findings have reported EphA2 receptor activation by soluble ephrin-A1 monomers that were released through membrane proteolytic cleavage from cancer cells, through unclear mechanisms[23,24].

Early crystallography studies of ephrin/Eph complexes have revealed hetero-tetramers formed by EphB2 and ephrin-B2 homodimers[25], as well as hetero-dimers of EphB2–ephrinA5 and EphB4–ephrin-B2[9,26]. Similar structures were later identified for EphA2 and ephrin-A1/A5 complexes[27–29]. These data contributed to the working ligand- and kinase-dependent Eph signaling model of which formations of ephrin-Eph hetero-dimers and hetero-tetramers lead to subsequent lateral assembly of higher-order clusters that can contain unliganded receptors[6,20,29] (Figure 1). The exact mechanisms underlying the stages of dimerization and tetramerization are still poorly understood. Nevertheless, there is a general consensus that tetramerization is the minimal unit for signal amplification leading up to functional cellular outcomes[18]. Interestingly, intra-class Eph receptors show unique clustering behaviors as evidenced by oligomeric versus array-like configurations in EphA4 and EphA2 clusters respectively[30]. In addition, EphA2 receptors can assemble into unliganded dimers in transfected human embryonic kidney (HEK293T) cells[31]. Signal termination is mediated by the *trans*-endocytosis of the large clusters in either ephrin or Eph-expressing cell[32]. This process involves proteolytic cleavage of Eph or ephrins by metalloproteases and γ-secretases at the cell membrane. In

particular, a disintegrin and metalloprotease domain-containing protein 10 (ADAM10) associates with EphA receptors and cleaves the ephrins interacting in *trans*. This results in membrane internalization of the complex containing the receptor and the ligand extracellular domains[33].

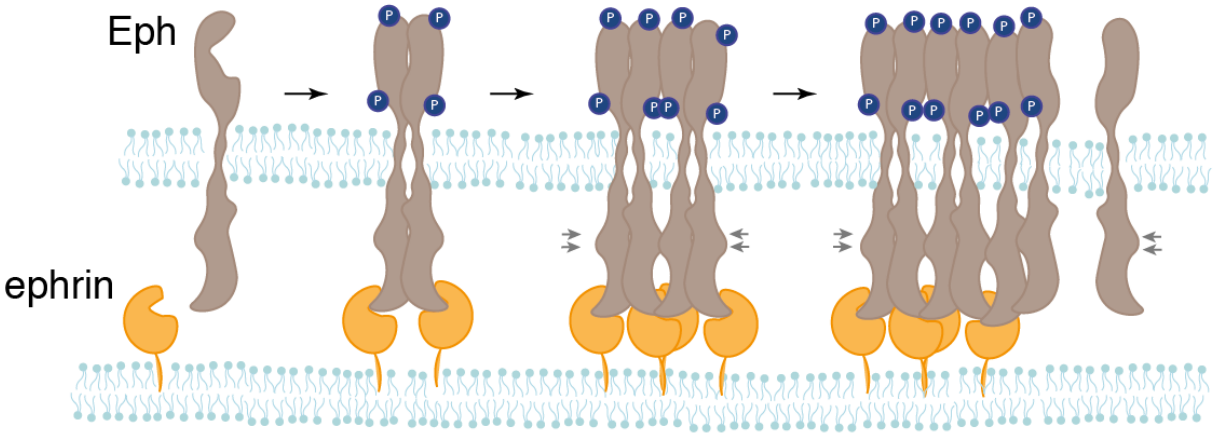

Figure 1. The proposed working model of Eph receptor activation. A single ephrin ligand binding to a Eph receptor triggers receptor conformation change and dimerization. Two Eph-ephrin dimers form a tetramer which induces strong receptor phosphorylation (blue circles). The tetramers can further form larger assemblies by recruiting ligand-bound and unliganded Eph receptors.

There has been compelling evidence demonstrating the importance of size, composition and spatial organization of ephrin-Eph clusters in Eph signaling strength and overall cellular responses. Experiments using synthetic dimerizers found EphB2 oligomers with higher receptor autophosphorylation levels than dimers and EphB-related cytoskeleton collapse responses from small clusters[34]. These responses were found correlated to the composition of oligomers versus dimers within signaling clusters[34]. Restriction of lateral transport and assembly of EphA2 clusters by physical patterns on supported lipid bilayers led to reduced recruitment of effector proteins, altered actin cytoskeleton and inhibition of ephrin *trans*-endocytosis[35,36]. Similarly, spatial modulation of EphB4 signaling using these patterned substrates disrupted cluster formation and inhibited neural stem cell differentiation[37]. Also, stimulation of neural stem cells with multivalent ephrin-B2 conjugates potently enhanced transcriptional activation of neuronal differentiation[38]. Furthermore, DNA origami nanofabrication of varying ephrin-A5 nanoscale patterns modulated EphA2 phosphorylation levels and invasiveness of human breast cancer cells[39]. Overall, these studies strongly suggest

that ephrin/Eph receptor signaling is regulated by its ability to spatially cluster at the cell-cell interface, in turn, eliciting a diverse plethora of functional outcomes.

1.2.2 Eph receptor signaling

Clustering of Eph receptors triggers autophosphorylation of tyrosine residues in the receptor juxtamembrane region, kinase domain and sterile alpha-motif domain[6]. The phosphotyrosines serve as docking sites for multiple SH2-domain adaptor proteins, which may be phosphorylated by the kinase domain[40]. Depending on the cell type, context and type of ephrin/Eph involved, these adaptors include the non-catalytic region of tyrosine kinase (NCK), chicken tumor virus number 10 regulator of kinase (CRK), phosphoinositide 3-kinase (PI3K) and Src family kinases which regulate the activity of many downstream signaling pathways that control cell adhesion and cytoskeleton organization[6]. The major pathways are the Ras homolog (Rho) family of guanine triphosphate (GTP)ases and Ras-mitogen-activated protein kinases/extracellular signal-regulated kinases (Ras-MAPK/ERK) pathways[40]. For instance, EphA2 activation suppressed MAPK signaling in endothelial and epithelial cells by growth factor receptor signaling such as epidermal growth factor (EGF), preventing cell proliferation[41]. In addition, EphB2-induced downregulation of GTP-bound Ras led to subsequent inhibition of Ras-MAPK pathway in neuronal cells, inducing neurite retraction[42].

1.2.3 EphA2 dysregulation in cancer

Among all the Eph receptors, EphA2 has the strongest association with cancer progression due to its aberrantly high expression in multiple cancer types[5,43]. These include cancer cell lines and solid tumors like breast, ovarian, melanoma, pancreas and glioblastoma associated with high metastatic potential, poor prognosis and patient survival[43]. Early *in vitro* work found that EphA2 overexpression is sufficient to transform non-malignant human breast epithelial cells to a malignant phenotype of high metastasis potential[44]. Moreover, EphA2-deficient tumors from breast cancer mouse models have reduced cell invasion and metastasis[45]. Paradoxically, EphA2 signaling in cancer not only has oncogenic but also tumor suppressive effects, possibly due to ligand-independent and ligand-dependent mechanisms[5,15]. Ligand-mediated activation of EphA2 inhibits integrin, Ras-MAPK and Rho GTPase activation, consequently suppressing cell adhesion, migration and proliferation[21,41,46]. Furthermore, the *EphA2* gene was found to be transcriptionally regulated by the p53 family of tumor suppressors and induced apoptosis when overexpressed[47]. Emerging evidence has shown that EphA2 overexpression is often accompanied with low expression of ephrin-A1 (cognate ligand of EphA2) in breast cancer cells and glioblastoma multiforme (GBM)[24,48,49]. This inverse expression pattern is suggested

to be mediated through an active Ras-MAPK pathway that is often dysregulated in cancer[50]. Ephrin activation of EphA2 can induce suppression of the MAPK pathway by a negative feedback inhibition of Ras activity, downregulating EphA2 protein expression[50]. However, this negative feedback regulation was not seen in MDA-MB-231 breast cancer cells[50], which have a constitutively active MAPK due to *KRAS* and *BRAF* gene mutations[51]. The tumor suppressive and oncogenic functions of EphA2 may also be explained by its signaling crosstalk with the PI3K-AKT pathway. Phosphorylation by AKT of a serine residue (S897) in EphA2 without ligand binding resulted in increased migration and invasion of glioma cells and stem cells, an effect which was reversed by ephrin-A1-EphA2 activation[15,52]. However, the S897 phosphorylation can also be induced by other kinases like protein kinase A and p90 ribosomal S6 kinase[53,54], further highlighting complex interplay of EphA2 with other signaling networks. Therefore, modulating the balance between EphA2 ligand-dependent and ligand-independent pathways may be useful to enhance tumor suppression or downregulate tumor-promoting signals for cancer therapy.

1.3 T-CELL SIGNALING

T cells are the crucial players of the body's adaptive immune system, involved in the cell-mediated immune response against a chronic infection/inflammation. T cells use their cell surface receptors, the T-cell receptor (TCR), to recognize self-derived or foreign peptide fragments that are bound to cell surface molecules called the major histocompatibility complex (MHC) expressed on their target cells. The latter can be either infected nucleated cells or professional antigen-presenting cells (APCs) which includes B cells, macrophages and dendritic cells. The TCR complex consists of the TCR antigen recognition α and β or γ and δ heterodimer chains in a non-covalent assembly with six cluster of differentiation 3 (CD3) adaptor proteins; CD3ε–CD3δ, CD3ε–CD3γ and CD3ζ–CD3ζ[55,56]. The TCR heterodimer has no intrinsic catalytic activity and relies on the CD3 cytoplasmic domains containing immunoreceptor tyrosine activation motifs (ITAMs) for signal transduction[57]. Briefly, recognition and binding of peptide-MHC (pMHC) by the TCR heterodimer chains lead to ITAM phosphorylation by lymphocyte-specific protein tyrosine kinase (LCK) and recruitment and activation of zeta-chain-associated protein kinase 70 (ZAP-70)[58,59]. Activated ZAP-70 phosphorylates the scaffold protein linker of activated T cells (LAT) which recruits multiple signaling effectors that trigger activation of downstream pathways such as calcium flux and nuclear factor-κB (NF-κB) signaling. Calcium signaling leads to nuclear translocation and activation of the nuclear factor of activated T cells (NFAT). In addition to the TCR-pMHC interaction, engagement of T cell costimulatory receptors such as CD28 is required to elicit a

functional immune response. By binding to CD80/86 on APCs, CD28 costimulation activates PI3K/AKT and MAPK pathways which leads to the formation of the activator protein 1 (AP1) complex in the nucleus[60]. The combined activities of NFAT, AP1 and NF-κB transcription factors activates gene transcription such as interleukin-2 (IL-2).

1.3.1 T-cell immunological synapse

The area of contact between a T cell and an APC was first described as the immunological synapse[61,62], defined as a bull's eye-like structure of distinct protein patterns[63,64]. These patterns were described as supramolecular activation clusters (SMACs) which are organized as a TCR-rich central core (cSMAC) surrounded by a peripheral SMAC (pSMAC) of lymphocyte function-associated antigen 1 (LFA-1) integrins and talin cytoskeletal proteins and a distal SMAC (dSMAC) of actin and CD45 tyrosine phosphatases[63,65] (Figure 2). It is important to note that this particular synaptic structure is not universal to all interfaces between T cells and their target cells. The synaptic architecture varies depending on the type of T cell and APC as well as the overall cellular context. For example, multiple TCR-rich cSMACs have been reported in T cell contacts with dendritic cells[66,67]. Despite this, the prototypical bull's eye pattern immune synapse has provided a spatial context for our understanding of T cell receptor signaling.

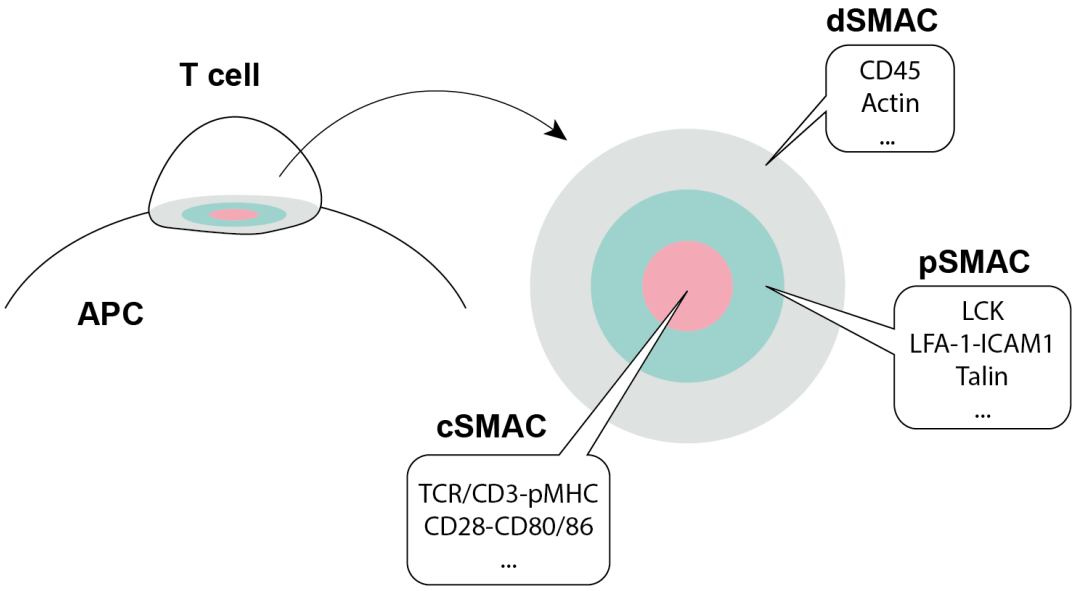

Figure 2. A simplistic illustration of the bull's eye pattern of the immunological synapse. Figure adapted from Yu *et al*[68].

1.3.2 TCR organization and signaling in the immunological synapse

The use of supported lipid bilayers as an *in vitro* reconstitution model has been instrumental in characterizing the underlying processes of the immunological synapse. This approach which

was pioneered by Dustin and colleagues, allows visualization of T cell interactions with proteins such as the peptide-MHC (pMHC) and LFA-1 binding intercellular adhesion molecule 1 (ICAM-1) attached on a planar lipid bilayer surface[64,69]. As these proteins linked to the lipids in the bilayer are highly mobile, they allow for movement of cell surface receptors following ligand binding. Total internal reflection fluorescence microscopy (TIRFM) is widely used to interrogate the molecules at the cell-bilayer interface. Using this imaging method, formation of TCR-pMHC microclusters was observed within 5 seconds of cell-bilayer contact[70]. It was estimated that each microcluster contains 40 – 150 TCR molecules in a 0.35 – 0.5 μm^2 area[70,71].

Most of these early TCR microclusters are colocalized with other TCR signaling proteins such as TCR co-stimulatory protein CD28, LCK, ZAP-70, LAT and adaptor protein SH2 domain-containing leukocyte protein of 76 kDa (SLP-76)[70–72]. Activated TCR signaling is indicated by phosphorylated ZAP-70 and tyrosine phosphorylation in most of the TCR microclusters and increased intracellular calcium[70,71]. As the cell spreads on the bilayer, newly generated TCR microclusters in the periphery are strongly associated with these activated kinases[70]. Concurrently, the T cell integrin LFA-1 bound to ICAM-1 on the bilayer are organized in microclusters spatially distinct from the TCR microclusters[73]. After 5 minutes of contact, most TCR and LFA-1 microclusters are centripetally transported by filamentous actin to form the cSMAC and pSMAC respectively[70,71,73,74]. TCR signaling is sustained by the continuous generation of TCR microclusters in the cell periphery associated with ZAP-70 and SLP-76 and their dissociation in migrating TCR microclusters to the synapse center[70]. In addition, CD28 proteins are segregated from these TCR microclusters and are translocated to a separate domain proximal to the TCR-rich cSMAC[72]. This led to a notion that TCR signaling is activated and maintained by the TCR microclusters and that the cSMAC is associated with TCR signal downregulation by TCR internalization and ubiquitin-mediated degradation[74–76]. This was supported by experiments which showed that peripheral TCR microclusters remain phosphorylated when constrained by chromium patterns on a supported lipid bilayer, while TCR microclusters in the center are unphosphorylated[77]. Furthermore, it has been shown that TCR-enriched microvesicles are formed in the cSMAC and released extracellularly to activate B cells[78]. This is in agreement with prior reports showing termination of TCR signaling in the cSMAC through the segregation of TCR microclusters into vesicular bodies[70,74]. However, the cSMAC can become the site of sustained TCR signaling following stimulation by weak pMHC agonists[79]. Based on this evidence, the spatial organization of TCRs and its signaling molecules not only regulates downstream signaling but is also highly dynamic and adaptable to the signaling context.

With the advent of super-resolution microscopy, further insights into the nanoscale organization of TCR and its signaling partners have been discovered. Using photoactivatable localization microscopy (PALM), TCR and LAT were found on membrane sheets of quiescent T cells as spatially distinct nanoclusters that concatenated upon TCR activation[80]. Combination of PALM and direct stochastic optical reconstruction microscopy (dSTORM) showed increased molecular density of TCR-CD3ζ nanoclusters and colocalization with phosphorylated ZAP-70 and LAT upon TCR stimulation[81]. Furthermore, TCR-CD3ζ clustering was demonstrated to be independent of CD3ζ phosphorylation as CD3ζ ITAM mutants retained clustering ability when stimulated[81]. *In situ* evidence of preclustered TCRs on naïve T cells and microcluster formation after T-cell activation in mouse lymph node tissues was also reported using dSTORM and light sheet microscopy[82]. However, others have argued that TCRs do not reside in pre-assembled nanoclusters but instead exist as monomers that are randomly distributed on non-activated T cells[83,84]. While it is unclear whether TCRs are organized in nanoclusters before engaging with pMHCs, collective evidence indicates that the spatial reorganization of pMHC-engaged TCRs into clusters is important for signal activation and propagation[70,74,77]. In addition, it has been shown that agonistic antibodies (anti-CD3 antibodies) or multivalent pMHC assemblies are needed to induce TCR clustering and *in vitro* T cell activation[85–87]. Soluble pMHC monomers bind but do not elicit TCR activation unless they are attached to a surface[88,89] while soluble pMHC dimers are able to activate T cells[90,91].

1.3.3 PD-1 immune checkpoint

T-cell signaling involves the TCR-pMHC ligation coupled with multiple receptor-ligand interactions within the immunological synapse. These interactions provide either positive costimulatory or negative coinhibitory signals that regulate T-cell signaling. One of the negative regulators is the Programmed Death 1 (PD-1) receptor and its ligands PD-L1 (B7-H1) or PD-L2 (B7-DC)[92–95]. PD-1 acts as an "immune checkpoint" to regulate effector T-cell responses and maintain peripheral immune tolerance[96]. The role of PD-1 in peripheral tolerance was first discovered when *Pdcd1* (which encodes for PD-1) gene knockout mice developed autoimmune diseases[97,98]. PD-1 is expressed in activated T cells upon acute antigen stimulation and then downregulated after antigenic clearance[99,100]. In contrast, PD-1 expression is sustained at high levels in T cells exposed to prolonged antigenic stimulation in chronic inflammation[100]. These T cells progressively become dysfunctional or "exhausted", exhibiting loss of effector functions including cytokine and chemokine production as well as upregulation of other co-inhibitory markers[101,102]. This is observed in tumor-infiltrating T cells in cancers including ovarian[103], breast,[104] and melanoma[105]. Moreover PD-L1 expression is induced in the pro-

inflammatory tumor microenvironment[96]. Thus, blocking PD-1 signaling would reinstate the T cell anti-tumor response[106,107]. In recent years, this approach has achieved tremendous clinical success as one of the immune checkpoint blockades in cancer immunotherapy, culminating in the Nobel Prize in Physiology or Medicine in 2018[108].

1.3.4 PD-1 in the immunological synapse

PD-1 was first reported to localize in the immunological synapse of T cells and dendritic cells[109]. Later studies using reconstituted supported lipid bilayers observed formation of PD-1 microclusters upon PD-L1 binding[110–112]. At initial cell-bilayer contact, the PD-1 microclusters are mostly colocalized with the TCR microclusters but strongly colocalized with CD28 microclusters[110,111]. As the cSMAC is formed, PD-1 molecules are organized together with CD28 molecules around the cSMAC, segregated from the TCR-rich core[110,111]. Upon PD-L1 binding, LCK-mediated phosphorylation of the PD-1 cytoplasmic domain occurs at the immunoreceptor tyrosine-based switch motif (ITSM) and immunoreceptor tyrosine-based inhibitory motif (ITIM). This triggers the recruitment of Src homology 2 domain–containing tyrosine phosphatase 2 (SHP2)[110,111,113](Figure 3). PD-1 negative suppression of T-cell signaling was observed by the recruitment of SHP2 in the early PD-1 microclusters and dephosphorylation of TCR-CD3ζ and CD28 molecules[110,111]. Recently, it has been shown that SHP2 induced PD-1 intracellular dimerization by binding to phosphotyrosines of the ITSMs of two PD-1 proteins[114]. While SHP2 is considered the primary mediator for PD-1 inhibitory effects, it appears that PD-1 can modulate T-cell signaling through SHP2-independent mechanisms[115–117]. The underlying mechanisms of how PD-1 signaling negatively regulates T-cell activation have been actively debated. Some studies have reported that PD-1 suppresses signaling through the TCR-CD3 complex[110,113,118], whereas others have argued that the CD28 pathway is preferentially targeted by PD-1[111,116]. In addition, CD28 costimulation is crucial for restoring T-cell proliferation after PD-1 blockade during chronic infections[119]. Interestingly, it was reported in the absence of CD28 costimulation, liganded PD-1 resided with another T-cell costimulatory receptor CD2 in the edge of the immunological synapse and reduced CD2 costimulation effect on TCR signaling[120]. This suggests an alternative mechanism of PD-1 negative regulation on T-cell signaling. While most studies focus on the PD-L1/PD-1 signaling in *trans*, a recent study showed that *cis* interactions of PD-1 and PD-L1 can occur in APCs to prevent binding of PD-L1 to PD-1 on T cells[112]. These evidences highlight the complexities of PD-1 signaling, making it difficult to draw the exact mechanisms of action by which PD-1 inhibits T-cell activation.

Based on structural and biophysical studies, PD-1 is expressed as a monomer on the cell surface and forms a 1:1 complex with PD-L1[121,122]. Thus, PD-L1 dimerization induced by small molecule inhibitors prevent the binding of PD-L1 to PD-1 and this enabled *in vitro* T cell reactivation[123,124]. However, a recent report identified a secreted PD-L1 splice variant from tumor cells that was able to form homodimers, which inhibited *in vitro* T-cell functions more strongly than soluble PD-L1 monomers[125]. Therefore, it is unclear whether the spatial proximity of PD-L1 ligands contribute to PD-1 inhibitory effects of T-cell signaling.

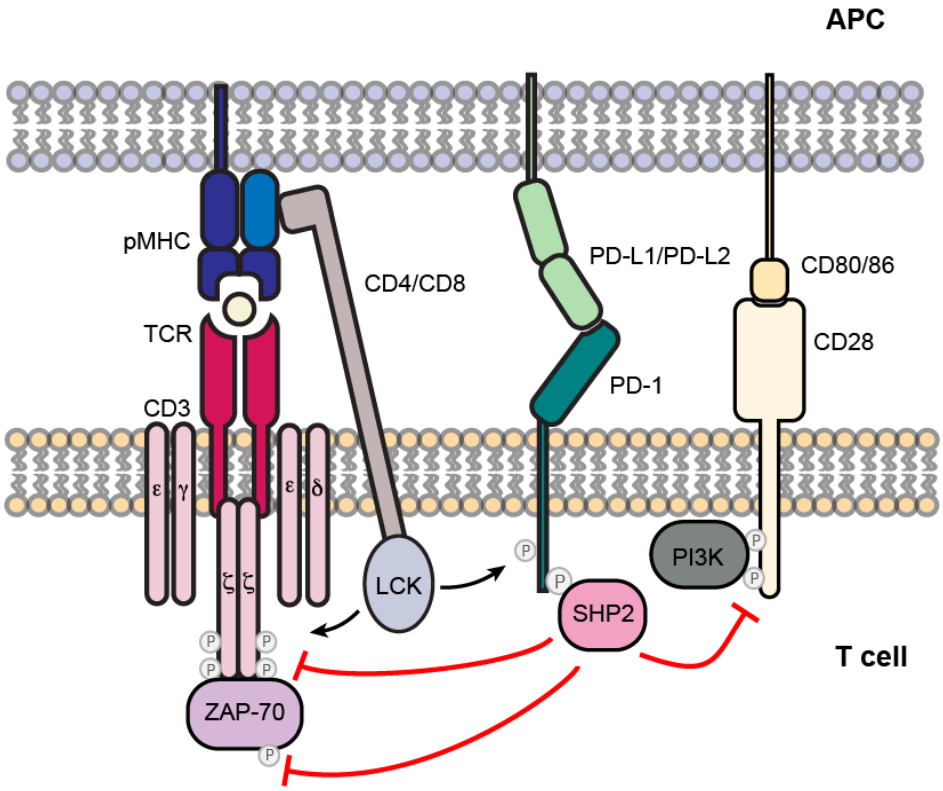

Figure 3. Brief schematic of the general notion of PD-1 signaling mechanism. T cell activation is initiated by pMHC-TCR binding and CD28 co-stimulation. PD-1 becomes expressed and binds to PD-L1/L2 on APCs or tumour cells. LCK-mediated phosphorylation at ITIM and ITSM of PD-1 leads to recruitment of phosphatases, including SHP-2. SHP2 mediates dephosphorylation of CD3ζ, ZAP-70 and CD28, therefore counters the activation of T cell signaling. Inhibitory signals (red blocked arrows).

1.4 DNA ORIGAMI

DNA origami is a technique that uses DNA as a structural material to drive self-assembly of 2D and 3D structures with nanoscale precision and programmability. First demonstrated by

Paul Rothemund in 2006, the technique involves mixing of a long circular single-stranded DNA ("scaffold"), usually obtained from the M13 bacteriophage, with many short single-stranded oligonucleotides ("staples")[126]. The staples are designed to bind complementarily to specific regions of the scaffold. Thus, this folds the scaffold into a predefined structure analogous to the art of paper folding (hence the name "DNA origami") (Figure 4).

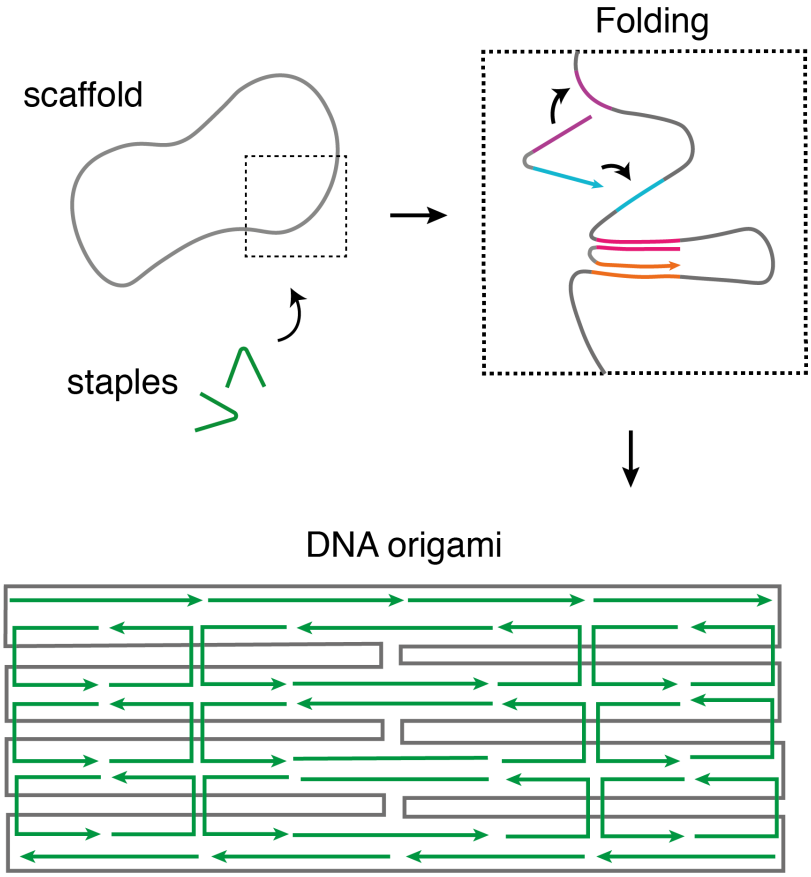

Figure 4. Principle of the DNA origami technique.

Since Rothemund's work on 2D sheets of monolayered DNA helices, the technique has rapidly developed to build 3D objects of any arbitrary shape including boxes with controllable lids[127], monolithic constructs[128] and curved structures[129130]. The early generation 3D structures were produced by closely packing bundles of DNA double-helices in honeycomb or square lattices[128,129,131,132]. DNA origami design with these geometries can be performed using the computational software caDNAno and model prediction tool CanDo[131,133]. However, the approach of densely packing of DNA helices uses more scaffold material and thus limits the dimensions of structures that can be constructed. More importantly, high cationic strength conditions are required to neutralize the electrostatic repulsion between the closely packed helices to prevent structure disintegration. To circumvent these caveats, new strategies based on wireframe designs have been developed to construct complex 2D and 3D polyhedral

structures[134–138]. The sparse wireframe geometries maximize the scaffold length, giving rise to larger surface areas. Furthermore, the structures can be folded and remain stable in physiological salt conditions[134], which makes them ideal for biomedical applications.

1.4.1 DNA origami as a tool for creating nanoscale patterns

The power of DNA origami is its spatial addressability which stems from the well-defined double helical geometry of DNA and the unique sequence of every staple and their specific positions in the final construct. The B-form DNA is commonly found in living cells and has a right-handed helix of a diameter of ~2.4 nm and a complete helical turn of ~3.4 nm for every 10.5 base pairs (bp)[139]. In honeycomb-based DNA origami constructs, crossovers from either the scaffold or staple strand connect neighboring DNA double helices. This creates sites of regular spacing of ~7 nm (21 bp) along the helical direction for functionalization[131]. By modifying individual staple strands, this enables positioning of diverse molecules including RNA[140], proteins[141–143], nanoparticles[144] and quantum dots[145], with nanometer precision. Hence the DNA origami method has been used extensively to produce nanoscale patterns in various applications. These include nanofabricated scaffolds for synthesis and assembly of nanoparticles[146,147], studying of biomolecular interactions and enzymatic cascades[142,148–150] as well as creation of nano-ruler standards for quantitative super-resolution imaging[151–153]. In addition, DNA origami nanostructures have been used to interrogate the spatial organization of membrane proteins in the contexts of ephrin-Eph signaling and viral antigenic-mediated B-cell receptor triggering[39,154].

Notably, DNA origami nanostructures as nanodevices for delivery of therapeutic molecules have been of major interest. Owing to its high structural programmability, DNA origami has enabled customized configurations for cellular delivery and controlled release of drug molecules[155,156]. *In vitro* and *in vivo* cellular targeting with various biomolecules including doxorubicin[156,157], immunostimulatory DNA[158], antibodies[155] and small interfering RNAs[159] loaded onto DNA origami nanostructures have been reported. Recent work has utilized DNA origami nanostructures loaded with tumor neoantigens as a cancer vaccine to trigger T-cell anti-tumor response in mouse cancer models[160]. Overall, the DNA origami technique have contributed to diverse applications from nanofabrication to *in vitro* and *in vivo* drug delivery and therefore holds immense potential for clinical use.

2 RESEARCH AIMS

The overall aim of the work in this thesis is to investigate the role of spatial organization of ligands on membrane receptor activation and downstream signaling responses by using DNA origami as a nanoscale patterning tool. This work addresses the spatial organization of ligands as an important biophysical factor in modulating receptor-mediated responses in two cellular signaling contexts. The following papers specifically aimed:

PAPER I – To investigate the role of the nanoscale spatial organization of ephrin-A5 ligands on EphA2 receptor activation and downstream transcriptional responses using ephrin-A5-patterned honeycomb DNA origami nanostructures.

PAPER II – To investigate the role of nanoscale spatial organization of PD-L1 on T-cell signaling and PD-1 distribution on the membrane using wireframe DNA origami flat sheets displaying PD-L1 at defined nanoscale distances.

3 MATERIALS AND METHODS

3.1 DNA ORIGAMI DESIGN AND FUNCTIONALIZATION

The work in this thesis employed two previously published designs of DNA origami nanostructures for nanoscale protein patterning[39,137]. In paper I, the DNA origami design described as a DNA nanocaliper, was an 18-double helix bundle arranged in a honeycomb lattice (Figure 5). In paper II, the DNA origami wireframe flat sheet design was used (Figure 6a). The single-stranded scaffolds for the honeycomb and wireframe designs are p7560 and p8064 respectively which are isolated from M13mp18 phage derivatives. In a "one-pot" reaction, the scaffold strands are mixed with a large molar excess of staples in a Tris-acetate-EDTA (TAE) buffer (pH 8) with 13 mM magnesium chloride ($MgCl_2$) for the DNA nanocaliper folding. The 1× phosphate-buffered saline (PBS) (pH 7.4) was used as a buffer for folding the DNA flat sheets. The DNA origami nanostructures were assembled through an annealing process on a thermal cycler that involves an initial heat denaturation step and subsequent gradual cooling over a 14-hour period. After folding, the assembled DNA origami nanostructures are separated from the excess staples by several rounds of diafiltration using Amicon® Ultra centrifugal filter columns.

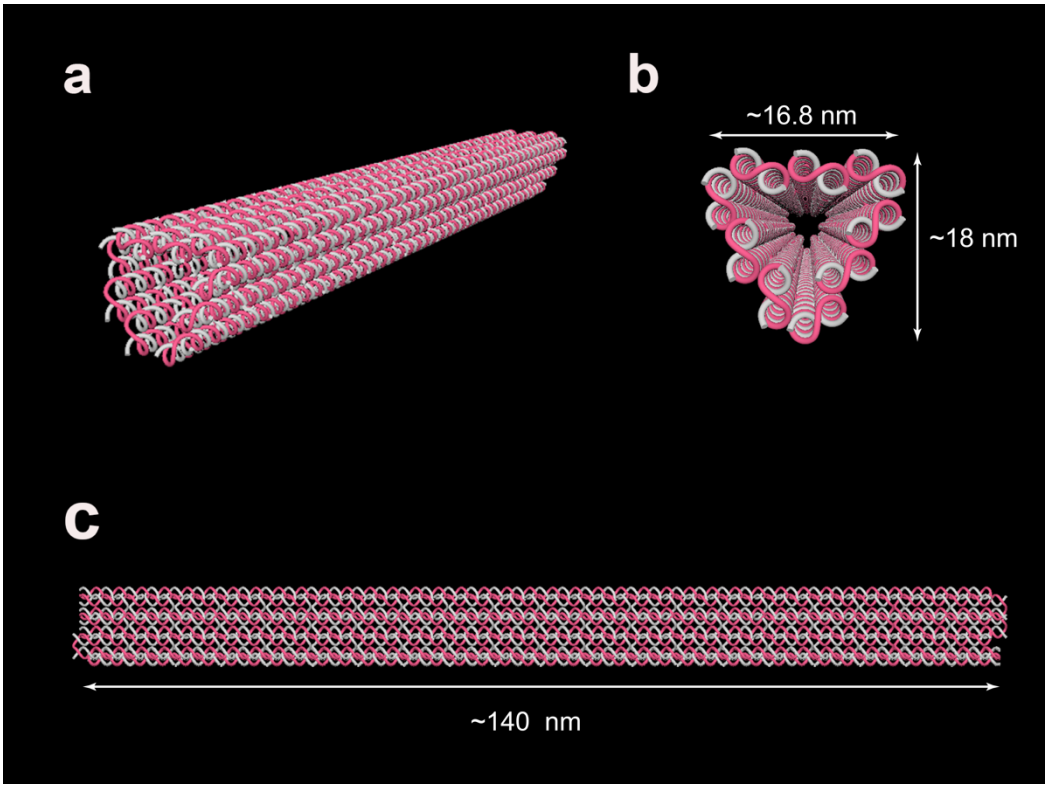

Figure 5. Stylized rendering of the DNA nanocaliper in three views (**a)** Perspective. (**b**) Front. (**c)** Side. The scaffold and staples are depicted as light grey and pink strands respectively.

To create sites for protein binding to the DNA origami, protruding staples containing a 5'overhang sequence are incorporated in the staple mix during the folding process (Figure 6b). Proteins that are conjugated to oligonucleotides would hybridize to the overhangs at these specific sites via complementary base pairing.

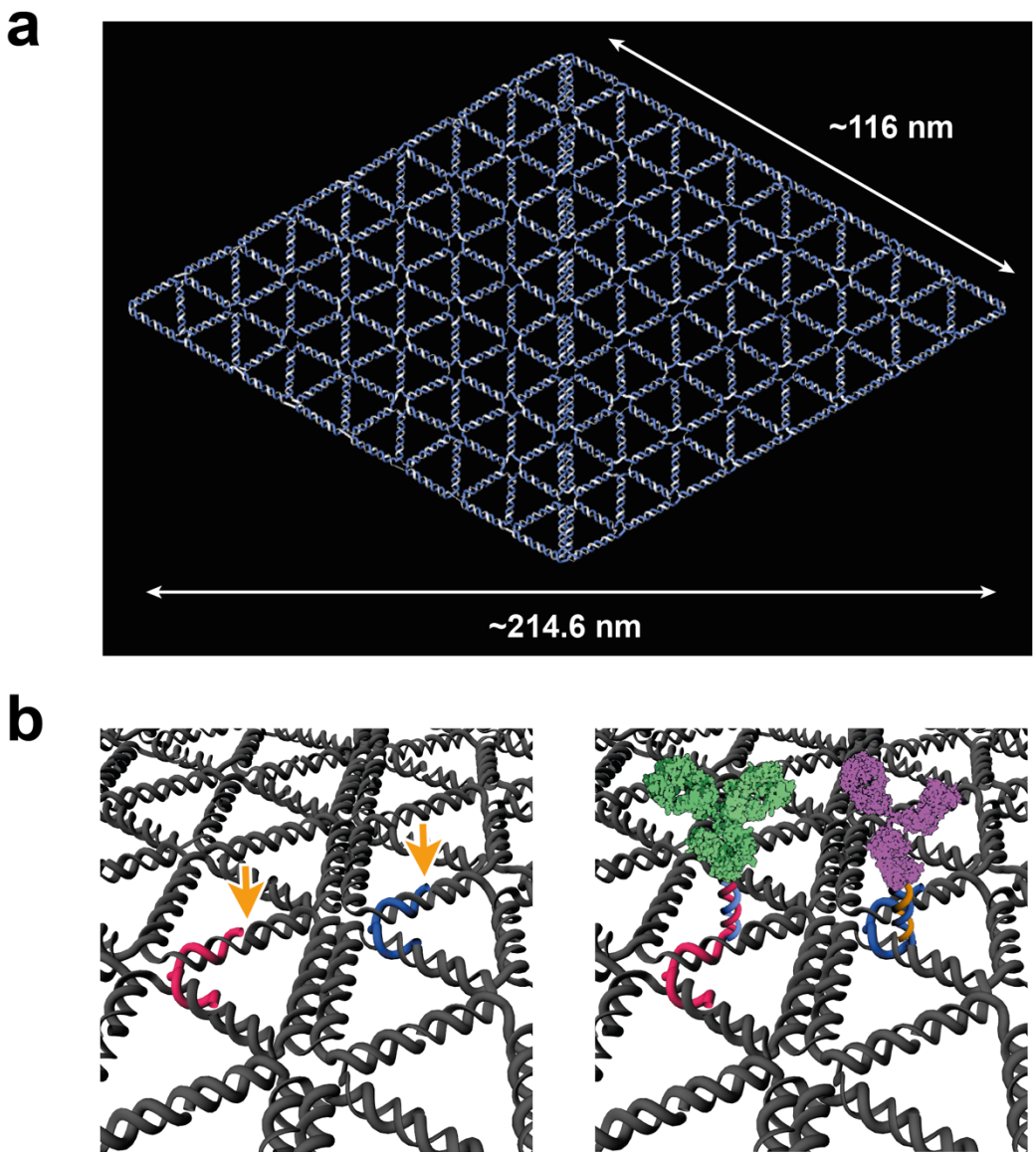

Figure 6. (**a**) Stylized rendering of the DNA wireframe origami flat sheet. The single-stranded scaffold strand (light grey) is folded by staple strands (blue) based on a triangulated mesh. **(b)** Illustration of protein binding to the DNA origami flat sheet. Two staples in the origami (left, orange arrows) are replaced with staples with a 19 or 21 bp extension at the 5' ends. This would allow hybridization by complementary base pairing with oligonucleotides that are conjugated to proteins (right).

Using this principle, protein patterns of different spatial distances and configurations can be assembled on the DNA origami. In paper I, the DNA nanocaliper was used to present four

different ephrin-A5 patterns. In paper II, T-cell activating DNA flat sheets were designed to present either the anti-CD3 antibody alone or a pair of anti-CD3 and anti-CD28 antibodies. The panel of PD-L1 flat sheets was designed with four different PD-L1 patterns. In addition, biotin-modified staples were introduced during the folding of the DNA flat sheets. This allows for immobilization of the protein-flat sheets on a streptavidin-biotin surface in subsequent cell stimulation experiments.

3.2 PRODUCTION OF PROTEIN-OLIGONUCLEOTIDE CONJUGATES

The oligonucleotides used for the protein conjugations are modified with an azide moiety at the 3' end. Conjugation of the 6-histidine (His_6)-tagged proteins (recombinant human ephrin-A5-Fc chimera and PD-L1) was adapted from a previously described histidine tag-specific polyethylene glycol (PEG) conjugation method[161]. The proteins are functionalized by crosslinking bis-sulfone-PEG_4-dibenzocyclooctyne (DBCO) molecules to the imidazole side chains of the histidine tags (Figure 7).

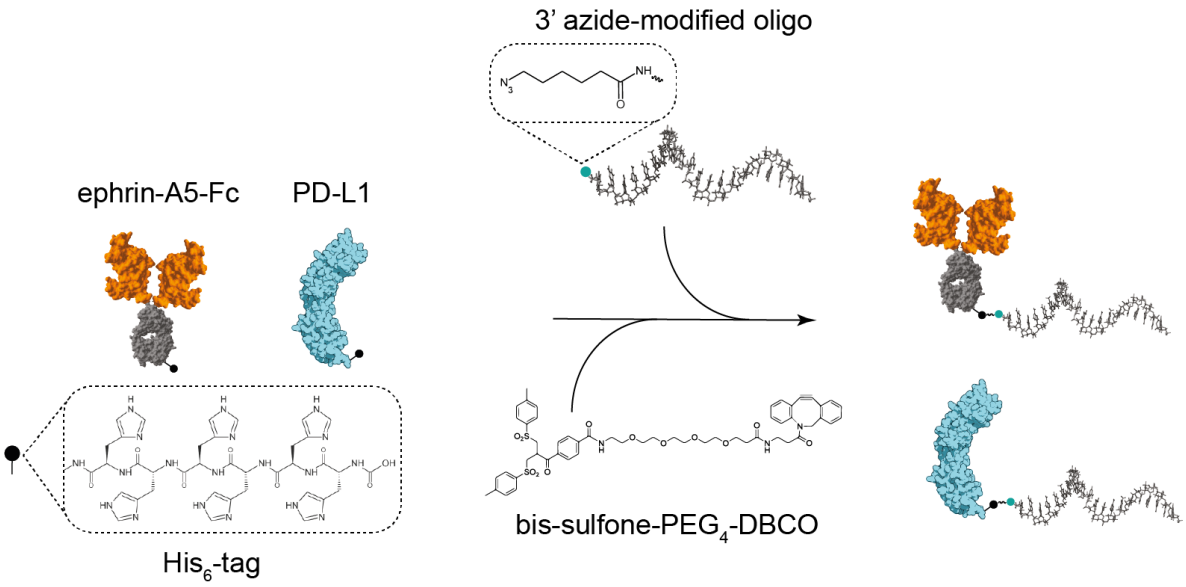

Figure 7. Schematic workflow of the histidine-tag directed conjugation of the ephrin-A5-Fc dimer and PD-L1 protein. The bis-sulfone-PEG_4-DBCO reagent is used for the incorporation of the DBCO moiety onto the proteins via their His_6-tags. The protein-oligonucleotide conjugates are formed via a copper-free click reaction of the DBCO group on the proteins and the azide-modified oligonucleotides.

As for the antibodies anti-CD3 and anti-CD28, they were functionalized by DBCO-*N*-hydroxysuccinimide (NHS) esters which targets primary amine groups, for example the side chains of lysine residues. The DBCO groups in the proteins then react to the azides in the

oligonucleotides via a copper-free click chemistry reaction. The resulting protein-oligonucleotide conjugates are purified using ultrafiltration to remove unconjugated oligonucleotides. The quality of protein-oligo conjugates was then assessed by 4-20% native polyacrylamide gel electrophoresis (PAGE) and silver staining after hybridization of fluorescently-labeled complementary oligonucleotides as well as reducing sodium dodecyl sulfate (SDS)-PAGE.

3.3 PRODUCTION AND CHARACTERIZATION OF PROTEIN-FUNCTIONALIZED DNA ORIGAMI

The protein-oligonucleotide conjugates are mixed with the assembled DNA origami at a 5-fold molar excess per binding site. Hybridization between the conjugates and the DNA origami was performed at 37°C for 1 hour, followed by rapid cooling to 22°C and then incubated for 14 hours. After incubation, the protein-DNA origami nanostructures are stored at 4°C. Excess protein-oligonucleotides are separated from the protein-DNA origami by gel filtration using Sepharose 6B resin packed columns (Figure 8). The quality and protein functionalization of the DNA origami were assessed by agarose gel electrophoresis. Despite their large size, the DNA nanocalipers migrate faster through the gel than the single-stranded scaffold due to the former's compact conformation.

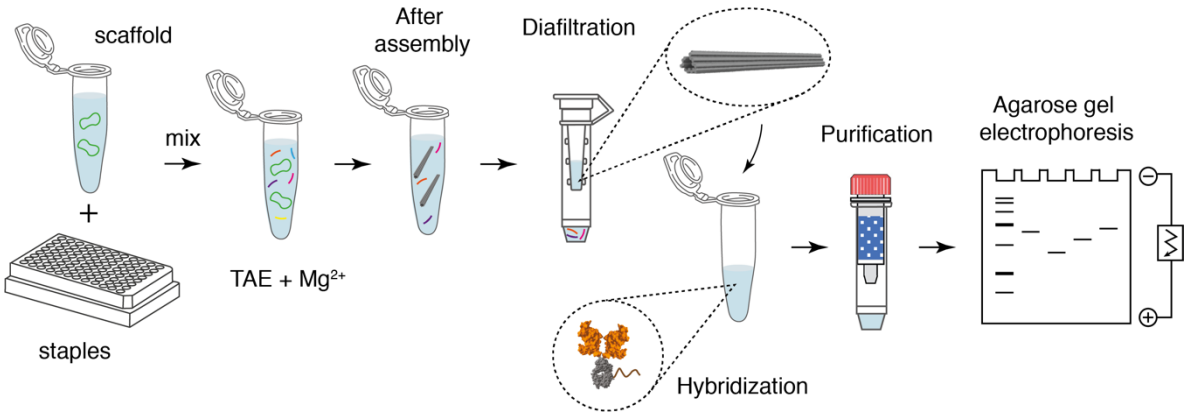

Figure 8. General overview of the production workflow of the protein-DNA origami nanostructures (ephrin-A5 DNA nanocaliper as an example). Folding of the DNA nanocaliper requires the presence of magnesium cations (Mg^{2+}). Diafiltration is performed to enrich the DNA nanocalipers and remove the unincorporated staples. The purified DNA nanocalipers are then mixed with the ephrin-A5-Fc-oligo conjugates for the hybridization reaction. The latter undergoes Sepharose 6B gel filtration to remove the non-hybridized conjugates and then assessed by agarose gel electrophoresis.

The gel migration distances were also used to determine whether the nanocalipers contain the ephrin-A5-Fc dimers. On the other hand, wireframe flat sheets migrate slower than the scaffold strand, possibly due to its open conformation. The proteins on the flat sheets were detected by in-gel fluorescence from fluorescently-labeled antibody binding. Transmission electron microscopy (TEM) and atomic force microscopy (AFM) were used for imaging the DNA nanocalipers and the flat sheets respectively and to confirm the assembly of proteins according to design.

3.4 CELLULAR READOUT EXPERIMENTS

3.4.1 Paper I: *In situ* proximity ligation assay (PLA)

Human breast cancer cell line MDA-MB-231 and human patient-derived U3013 glioblastoma cells were seeded on glass coverslips 24 hours before treatment with ephrin-A5 nanocalipers. MDA-MB-231 cells were starved in reduced amounts of serum for 24 hours to decrease baseline phosphorylation levels. The cells were treated with the nanocalipers presenting ephrin-A5-Fc dimers of different distances in a PBS solution supplemented with 13 mM $MgCl_2$ and incubated for 15 and 30 minutes.

To detect EphA2 receptor phosphorylation, the cells were fixed and processed using the Duolink® PLA kit (Sigma-Aldrich) according to manufacturer's guidelines. This method is based on the principle of close proximity binding of anti-phosphotyrosine antibodies and antibodies that target the intracellular domains of EphA2 (Figure 9). This allows for a fluorescence-based quantitative readout of single events of EphA2 receptor tyrosine phosphorylation.

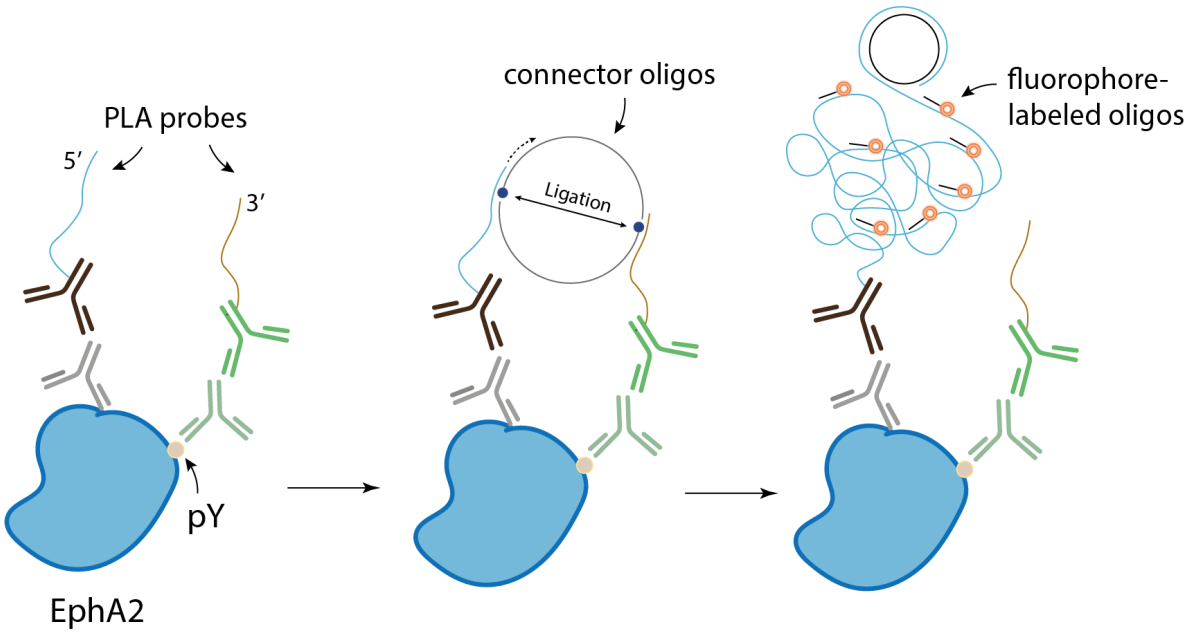

Figure 9. Schematic outline of the PLA to detect EphA2 tyrosine phosphorylation. First, two antibodies recognize the phosphorylated tyrosine residues (pY) and the cytoplasmic region of EphA2. These antibodies are targets for binding of secondary antibodies conjugated with oligonucleotides (PLA probes). If the PLA probes bind in close proximity (< 40 nm), this would guide two connector oligonucleotides with 5' phosphate ends (blue dots) to form a circular DNA structure by enzymatic DNA ligation. Rolling circle amplification (RCA) is initiated by the phi-29 DNA polymerase which uses an oligonucleotide of one PLA probe as a primer (dotted arrow). The oligonucleotide of the other probe contains a 2'*O*-methyl RNA modification at the 3'end, which blocks the polymerase from using it as a primer for the RCA. Using the circularized single-stranded DNA as a template, the polymerase generates a concatemer of multiple repeats that are complementary to the DNA circle template. Finally, the DNA concatemer is detected by complementary fluorescently-labeled oligonucleotides. Figure is adapted from the paper that showed the first demonstration of the *in situ* PLA technique[162].

3.4.2 Paper II: Luciferase reporter assay

To measure T cell activation in response to antibody and PD-L1 DNA origami flat sheets, a commercially available Jurkat T cell line constitutively expressing PD-1 and a nuclear factor of activated T cells (NFAT) response element-firefly luciferase gene reporter (BPS Bioscience) was used. The cells were stimulated by antibody and PD-L1 flat sheets coated on streptavidin-biotinylated bovine serum albumin (BSA) surface for 3 hours before cell lysis and luciferase activity measurements. Anti-CD3 and CD28 antibody-induced T-cell activation triggers expression of the luciferase protein via activation of NFAT and binding to the response

elements. The luciferase activity is quantified by the bioluminescence generated from the luciferase-driven catalysis of the luciferin substrate.

3.4.3 Paper II: Generation of PD-1-expressing T-cell model for super resolution microscopy

To investigate the PD-1 distributions on the cell membrane, Jurkat E6-1 cells were retrovirally transduced to express PD-1 fused with an intracellular SNAP-tag protein. The SNAP-tag is a 20 kDa mutant DNA repair enzyme O_6-alkylguanine-DNA alkyltransferase, which allows covalent labeling of benzylguanine-modified fluorophores to the protein. The SNAP-tag offers specific protein-labeling of organic fluorescent dyes which have higher photon-output and photostability than fluorescent proteins[163]. Moreover, the large size of fluorescent protein tags and their tendency to oligomerize reduce the precision of target protein localization. For this purpose, an 880 bp cDNA sequence encoding the human PD-1 (R&D Systems) was subcloned into the $pSNAP_f$ vector (New England Biolabs), as a fusion to the N-terminus of the SNAP-tag. Restriction enzymatic digestion was performed to obtain the PD-1-SNAP construct and then cloned into a murine stem cell retrovirus plasmid (pMSCV) containing the neomycin resistance gene (kindly given by Dr. Stephen L. Lessnick from Nationwide Children's Hospital). The retrovirus construct containing the PD-1-SNAP insert was sent to the Vector Facility in Lund University for retroviral vector production. Jurkat cells were retrovirally transduced at a multiplicity of infection (MOI) of 20 and then selected for G418 (neomycin analogue) antibiotic resistance. Single cells were isolated by the limiting dilution method to obtain a monoclonal cell population expressing the PD-1-SNAP-tag fusion protein. Surface expression of PD-1 was estimated by flow cytometry based on fluorescence quantitation with phycoerythrin-labeled anti-PD-1 antibodies and Quantibrite™ beads (BD Biosciences). In addition, PD-1 and SNAP expression were assessed by Western blot. The cells were further characterized for IL-2 expression by enzyme-linked immunosorbent assay (ELISA) when stimulated with antibodies anti-CD3 and CD28 and PD-L1 proteins.

4 RESULTS & DISCUSSION

4.1 PAPER I

4.1.1 Ephrin-A5 DNA nanocaliper production and characterization

We used the designs of the ephrin-A5 functionalized DNA nanocaliper as previously published[39] to study the effects of nanoscale spatial organization of ephrin-A5 on EphA2 receptor phosphorylation and transcriptional response. We adapted a polyhistidine tag-specific labeling approach for covalent conjugation of DNA to His_6-tagged ephrin-A5-Fc dimers. This method gives more control in the protein modification and minimizes interference in protein functionality from random labeling by primary amine or sulfhydryl group-based bioconjugation strategies. Based on the native polyacrylamide gel fluorescence and silver stain, two ephrin-A5-Fc-oligonucleotide products were detected with differing fluorescent intensities that suggest one or two oligonucleotides were coupled to the ephrin-A5-Fc dimer. More importantly, the in-gel fluorescence showed that the unincorporated azide-oligonucleotides were efficiently removed from the ephrin-A5-oligonucleotide conjugate reaction after diafiltration. The ephrin-A5-oligonucleotide conjugates were then incorporated to the DNA nanocalipers via hybridization to the protruding staples at different positions, producing a panel of nanocalipers that present one ephrin-A5 dimer (NC-0) or two dimers separated by 14.3 nm (NC-14), 42.9 nm (NC-40) and 101.1 nm (NC-100).

We verified the DNA nanocalipers functionalized with the ephrin-A5-oligonucleotide conjugates by agarose gel electrophoresis and TEM imaging (Figure 10). In the agarose gels, the ephrin-A5 DNA nanocalipers migrated at shorter distances than the non-functionalized DNA nanocaliper (NC-empty). In addition, DNA nanocalipers with two ephrin-A5 dimers (NC-14, NC-40 and NC-100) had shorter gel migration distances than the nanocalipers with one ephrin-A5 dimer (NC-0). We also confirmed binding of recombinant EphA2 proteins to the ephrin-A5 DNA nanocalipers by agarose gel electrophoresis.

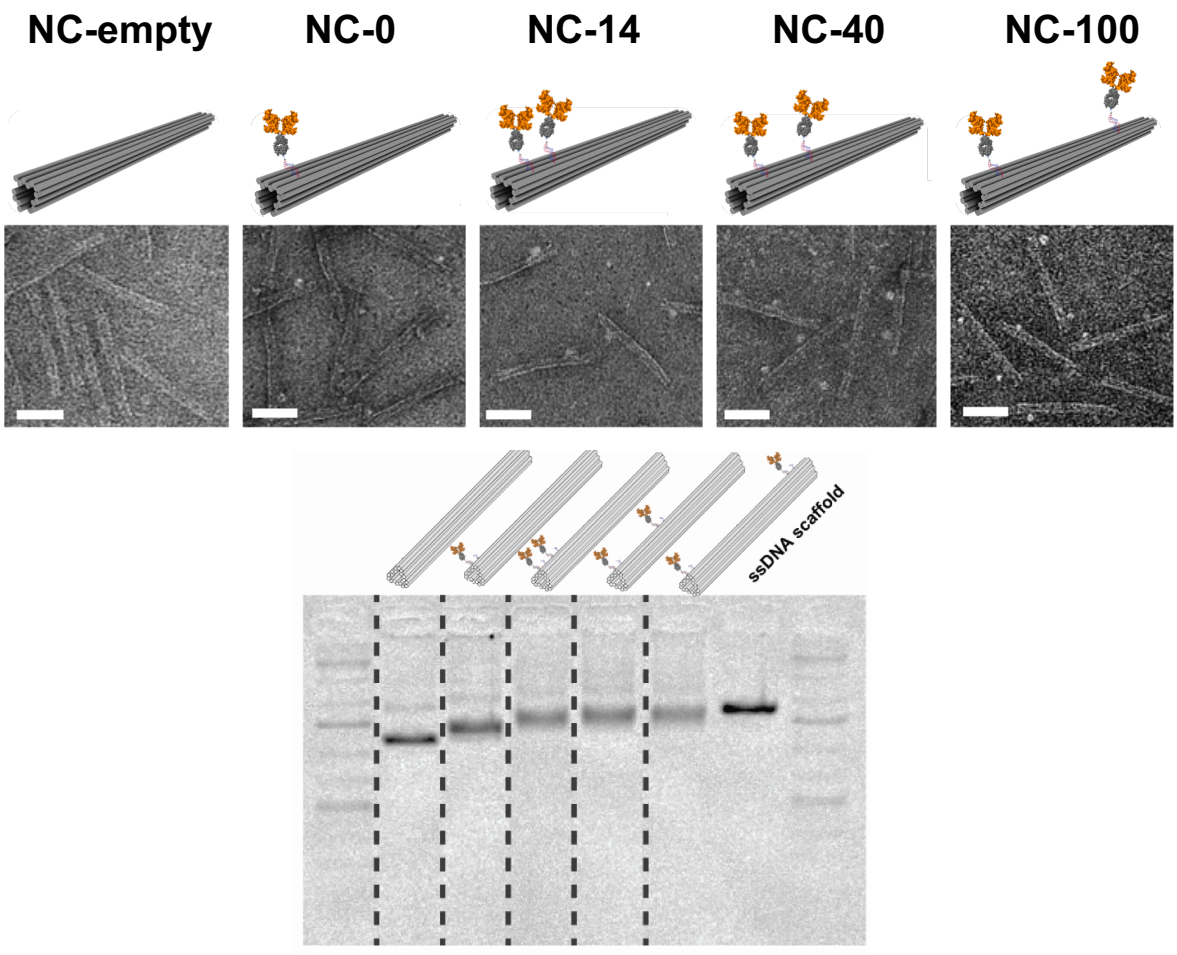

Figure 10. Respective TEM and agarose gel images of the DNA nanocalipers presenting ephrin-A5-Fc dimers at different positions.

4.1.2 EphA2 receptor activation is spatially regulated by ephrin-A5 DNA nanocalipers

Next, we investigated the effect of EphA2 receptor activation in MDA-MB-231 breast cancer cells and U3013 glioblastoma cells in response to stimulations by the different ephrin-A5 nanocalipers at two stimulation times. Using the PLA method, we observed increased EphA2 phosphorylation in MDA-MB-231 and U3013 cells after 15 minutes of stimulation by the ephrin-A5 DNA nanocalipers. At this timepoint, we observed that NC-40 and NC-100 induced the highest level of EphA2 phosphorylation in MDA-MB-231 and U3013 cells, respectively. In MDA-MB-231 cells, levels of EphA2 phosphorylation induced by NC-40 also significantly differed from those by NC-0 and NC-100. In U3013 cells, NC-100 induced differential EphA2 phosphorylation levels compared to NC-0, NC-14 and NC-40. After 30 minutes of stimulation, both cell types showed variable EphA2 phosphorylation levels, with only NC-40 inducing significant phosphorylation. Overall, these results suggest that EphA2 phosphorylation is regulated by ephrin-A5 spatial distribution at a short stimulation time (15 min).

4.1.3 U3013 cells showed more EphA2-associated transcriptional responses to "classical" EphA2 stimulation than MDA-MB-231 cells

The standard approach for *in vitro* Eph receptor clustering and activation involves pre-clustering of recombinant ephrin-Fc fusions by anti-Fc antibodies in solution before cell stimulation. This method yields a heterogeneous mixture of higher-order ephrin oligomers and therefore does not allow for control of ligand cluster sizes. We sought to understand the transcriptional profiles of MDA-MB-231 and U3013 cells after EphA2 activation with this method. For this purpose, we performed RNA-sequencing with low cell numbers (~400 cell equivalents) based on an adaptation of the Smart-seq2 protocol[164]. We observed that U3013 cells showed more EphA2-associated pathways that are significantly enriched compared to those found in MDA-MB-231 cells. This indicates that the former is more transcriptionally responsive to EphA2 activation.

4.1.4 Divergence in the EphA2-associated transcriptional response to increasing ephrin-A5 spatial distance

As the U3013 cells are more responsive to EphA2 activation at the transcriptomic level, we further analyzed their transcriptome after cell stimulation with the different ephrin-A5 nanocalipers. Increasing ephrin-A5 dimer distances up to ~100 nm on the DNA nanocaliper (NC-100) increased the number of differentially expressed (DE) genes. This is accompanied by a decreasing percentage of DE genes overlapping with one or more nanocaliper data sets as the spatial distance between ephrin-A5 dimers increases. This spatially-induced divergence in EphA2 transcriptional response is supported by correlation analyses, which showed that the NC-40 and NC-100 induced EphA2 transcriptional responses that are distinct from those by NC-0 and NC-14 stimulation. Additionally, pathway enrichment analysis showed distinct significantly enriched pathways induced by the different ephrin-A5 nanocaliper conditions. Intriguingly, while NC-40 and NC-100 differed in their significantly enriched pathways, some of those are subsets of pathways triggered by antibody-clustered ephrin-A5 stimulation (Figure 11). Together, these results indicate that the spatial distance of ephrin-A5 dimers at the nanoscale modulates the EphA2 transcriptional network.

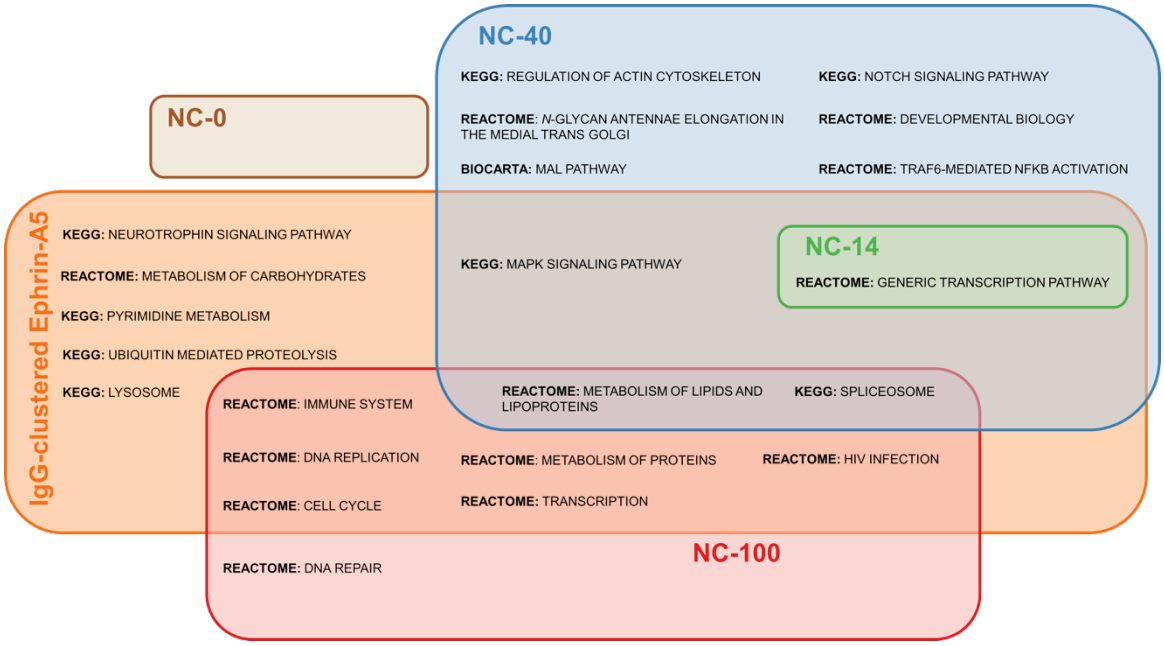

Figure 11. A Euler diagram illustrating the induced significantly enriched pathways between antibody-clustered ephrin-A5 and ephrin-A5 DNA nanocaliper stimulations.

4.2 PAPER II

4.2.1 Production of antibody- and PD-L1-patterned DNA wireframe origami flat sheets

For T cell activation, DNA wireframe origami flat sheets were functionalized with a single anti-CD3 antibody (FS-α-CD3) or anti-CD3 and CD28 antibodies (FS-α-CD3-CD28) (Figure 12). A panel of PD-L1-patterned flat sheets were constructed as follows; a single PD-L1 protein (FS-PD-L1) and two PD-L1 proteins separated by 13.6 nm, 43.5 nm and 202.3 nm (FS-PD-L1-13, FS-PD-L1-40 and FS-PD-L1-200).

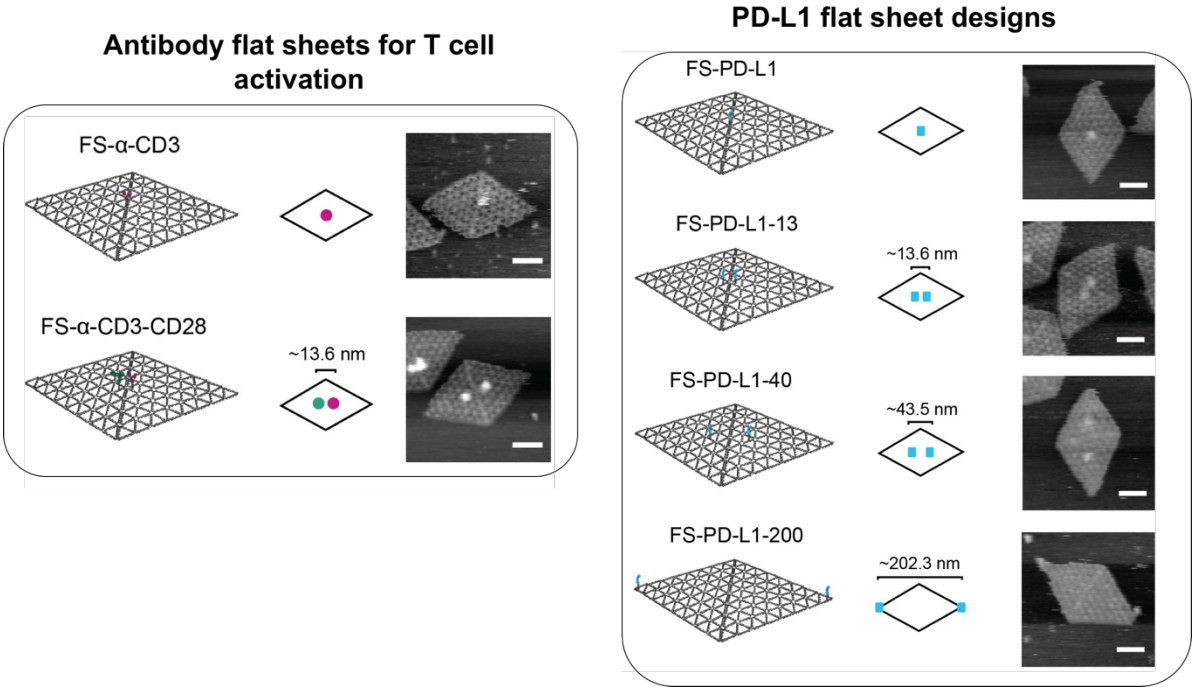

Figure 12. The antibody and PD-L1 flat sheet designs and their respective AFM images.

Using agarose gel electrophoresis, the protein-flat sheets showed no detectable difference in gel migration compared to flat sheets with no proteins attached (FS-empty). Hence, the protein-flat sheets were pre-mixed with fluorescently-labeled antibodies that recognize the antibody-Fc domains and PD-L1 proteins to allow for in-gel fluorescence detection. AFM imaging was performed to confirm the protein occupancy as designed, which was estimated to be about 40-65%. Additionally, surface plasmon resonance measurements validated the binding of PD-L1 flat sheets to PD-1 receptors.

4.2.2 Modulation of T-cell signaling and PD-1 clustering by PD-L1 spatial distances

PD-1-expressing Jurkat T cells with a NFAT-driven luciferase reporter were stimulated with antibody- and PD-L1-patterned flat sheets. We observed a significant decrease in antibody-induced NFAT-luciferase activity only when cells were co-stimulated with FS-PD-L1-200. Co-stimulation with flat sheets containing a single PD-L1 or two PD-L1 proteins spaced 13 or 40 nm apart did not result in a significant change in antibody-induced NFAT-luciferase activity. Furthermore, the reduction in NFAT-luciferase activity by FS-PD-L1-200 is dependent on the molar ratio of FS-PD-L1-200 to antibody-flat sheets, in which FS-PD-L1-200 at a 10-fold molar excess of the antibody-flat sheets was needed for significant change. Co-stimulation with FS-PD-L1-200 also led to a significant decrease in IL-2 gene expression in Jurkat T cells expressing PD-1 with a SNAP-tag (PD-1-SNAP). Analyzing the membrane distribution of PD-1 receptors in these cells by stimulated emission depletion (STED) imaging found an increase in the density of PD-1 clusters upon PD-L1 flat sheet stimulation. FS-PD-L1-200 and the antibody-flat sheet negative controls mostly triggered small PD-1 clusters (~50-100 nm) while FS-PD-L1-13 induced larger clusters (>100 nm). Together, these results show that the spatial organization of PD-L1 at the nanoscale regulates T cell signaling and PD-1 receptor cluster size.

5 CONCLUSIONS

This thesis presents a multidisciplinary body of work integrating DNA origami technology, next-generation sequencing, super-resolution microscopy and molecular biology techniques to examine the role of nanoscale spatial organization of ligands on ligand-receptor pathways in the contexts of cancer biology and immunology. We used the DNA origami technique as a nanoscopic tool to present ligands at precise nanoscale distances that would guide the organization of cell membrane receptors into defined configurations. In paper I, we demonstrated how the spatial organization at the cell interface contributes to the ensuing events in the ephrin-Eph signaling. We showed that the nanoscale spatial organization of ephrin-A5 dimers regulates early EphA2 receptor activity and downstream transcriptional responses. As Eph signaling is interweaved with pro-tumorigenic and tumor suppressive pathways, this complicates the development of effective anti-cancer agents against ephrin-Eph signaling. The knowledge gained from this study may provide a basis for new strategies to selectively target specific pathways in ephrin-Ephrin signaling for anti-cancer therapy.

The spatial organization of T-cell signaling proteins is a key biophysical regulator of signal transduction in the immunological synapse. As seen in paper II, we demonstrated that the spatial organization of PD-L1 controls T-cell signaling and functional response of IL-2 gene expression (paper II). This work highlights that the spatial organization of co-inhibitory proteins also contributes to signal regulation in the T-cell immunological synapse. The spatial organization of PD-L1/PD-1 may be used as a mechanical stimulus in new cancer immunotherapies to modulate T-cell activation and restore the anti-tumor immune response.

6 POINTS OF PERSPECTIVE

To understand the mechanism behind the spatial regulation of EphA2 transcriptional response, it would be interesting to examine how EphA2 clusters on the membrane upon binding to the ephrin-A5 nanocalipers. We hypothesize that NC-40 and NC-100 induce two sites of EphA2 receptor dimerization spaced 40 and 100 nm apart on the cell membrane that might initiate recruitment of more EphA2 receptors to the sites. It might be possible that the two EphA2 dimers merge into a large cluster, with NC-100 resulting in larger receptor cluster than NC-40. On the other hand, NC-14 may have introduced a single receptor cluster/oligomerization site due to the proximity of the two ephrin-A5 dimers. NC-0 with a single ephrin-A5-Fc dimer may have triggered dimerization of EphA2 receptors. As the starting EphA2 clustering sites are small, receptor clustering induced by NC-0 and NC-14 may take a longer time as compared to NC-40 and NC-100. This hypothesis may explain the observation of the diverging response of EphA2 signaling from the nanocaliper stimulations, with NC-100 inducing the largest response. Live cell imaging using super resolution microscopy techniques may shed light on the Eph receptor cluster formation as well as the kinetics in response to the different ligand nanoscale distances. The kinetics of the clustering can be used as a basis to elucidate the mechanisms with the transcriptional responses induced by the nanocalipers at different stimulation times.

The exact molecular mechanism underlying the regulation on T-cell activation by PD-L1 spatial distances requires further exploration. An in-depth investigation of the recruitment of PD-1 signaling adaptors SHP1/SHP2 in response to the PD-L1 flat sheets is essential to provide a better understanding of the spatial regulation induced by PD-L1. As PD-1 microclusters have been shown to strongly associate with CD28 receptor clusters on supported lipid bilayers in the literature, it would be worth investigating the spatial distance of PD-1 and CD28 receptors as well.

7 ACKNOWLEDGEMENTS

This thesis is the culmination of venturing into uncharted waters for over half a decade. I must admit that it has been a tumultuous experience, not because of the intellectual challenges one has to overcome but rather the amount of sheer perseverance needed. The work behind a PhD thesis cannot be completed by the sole effort of an individual. It is, in fact, the collective effort from the people behind that individual on this endeavor. Therefore, I thank the following people:

Ana 👩‍🔬 for giving me the opportunity to work in such a unique and ambitious multidisciplinary project. **Björn** 🧛 for being my co-supervisor and providing your DNA origami expertise. Importantly, I am grateful for the financial support from the **European Research Council Consolidator Grant, KID funding** and the **Knut and Alice Wallenberg Foundation** 💰

Toon 👨‍🔬 I believe that we work great together as a team 👉. Thank you for the massive support you gave all these years. Your openness of sharing protocols and knowledge and support in IT-related matters, (the now-defunct lab wiki, data servers and website) is truly appreciated. **Sijie** for bringing so much enthusiasm and good cheer. Your jovial spirit lights up the room ☺️. **Ki-Young** for your ingenuity 🤯 and strong work ethics. **Mahdi** who started the PD-1 project and gave me PhD advice right from the start 🙌. **Yang** 👦 Thanks for the collab and all the exchanges and discussions we had. Not to mention the help on the vHelix and Maya rendering and tolerating my horrendous Chinese as well 😬. **Christos**, I truly enjoyed our talks, it was comforting to have someone in the lab who listens and understands 👂. My mentor, **Benjamin**, the director of doctoral education in MBB, **Elias**, and admin **Victoria** for the help and support. My collaborators and co-authors **Dominik, Karen, Arne, Ilaria, Jonatan, Elena** and **Joel**. Also, **Javier** for the flow cytometry support during the early years of my PhD.

Last but not least, my family and friends back in SG, GAMXIA. And **Valdmortia** for keeping me sane and making our travels in 🇳🇴 and 🇫🇴 unforgettable #norgetwopointzero.

8 REFERENCES

(1) Manz, B. N.; Groves, J. T. Spatial Organization and Signal Transduction at Intercellular Junctions. *Nat. Rev. Mol. Cell Biol.* **2010**, *11* (5), 342–352.

(2) Bethani, I.; Skånland, S. S.; Dikic, I.; Acker-Palmer, A. Spatial Organization of Transmembrane Receptor Signalling. *EMBO J.* **2010**, *29* (16), 2677–2688.

(3) Casaletto, J. B.; McClatchey, A. I. Spatial Regulation of Receptor Tyrosine Kinases in Development and Cancer. *Nat. Rev. Cancer* **2012**, *12* (6), 387–400.

(4) Lemmon, M. A.; Schlessinger, J. Cell Signaling by Receptor Tyrosine Kinases. *Cell* **2010**, *141* (7), 1117–1134.

(5) Pasquale, E. B. Eph Receptors and Ephrins in Cancer: Bidirectional Signalling and Beyond. *Nat. Rev. Cancer* **2010**, *10* (3), 165–180.

(6) Kania, A.; Klein, R. Mechanisms of Ephrin-Eph Signalling in Development, Physiology and Disease. *Nat. Rev. Mol. Cell Biol.* **2016**, *17* (4), 240–256.

(7) Hirai, H.; Maru, Y.; Hagiwara, K.; Nishida, J.; Takaku, F. A Novel Putative Tyrosine Kinase Receptor Encoded by the Eph Gene. *Science* **1987**, *238* (4834), 1717–1720.

(8) Maru, Y.; Hirai, H.; Takaku, F. Overexpression Confers an Oncogenic Potential upon the Eph Gene. *Oncogene* **1990**, *5* (3), 445–447.

(9) Himanen, J. P.; Chumley, M. J.; Lackmann, M.; Li, C.; Barton, W. A.; Jeffrey, P. D.; Vearing, C.; Geleick, D.; Feldheim, D. A.; Boyd, A. W.; Henkemeyer, M.; Nikolov, D. B. Repelling Class Discrimination: Ephrin-A5 Binds to and Activates EphB2 Receptor Signaling. *Nat. Neurosci.* **2004**, *7* (5), 501–509.

(10) Kullander, K.; Butt, S. J. B.; Lebret, J. M.; Lundfald, L.; Restrepo, C. E.; Rydström, A.; Klein, R.; Kiehn, O. Role of EphA4 and EphrinB3 in Local Neuronal Circuits That Control Walking. *Science* **2003**, *299* (5614), 1889–1892.

(11) Boyd, A. W.; Bartlett, P. F.; Lackmann, M. Therapeutic Targeting of EPH Receptors and Their Ligands. *Nat. Rev. Drug Discov.* **2014**, *13* (1), 39–62.

(12) Yin, Y.; Yamashita, Y.; Noda, H.; Okafuji, T.; Go, M. J.; Tanaka, H. EphA Receptor Tyrosine Kinases Interact with Co-Expressed Ephrin-A Ligands in Cis. *Neurosci. Res.* **2004**, *48* (3), 285–295.

(13) Carvalho, R. F.; Beutler, M.; Marler, K. J. M.; Knöll, B.; Becker-Barroso, E.; Heintzmann, R.; Ng, T.; Drescher, U. Silencing of EphA3 through a Cis Interaction with

EphrinA5. *Nat. Neurosci.* **2006**, *9* (3), 322–330.

(14) Kao, T. J.; Kania, A. Ephrin-Mediated Cis-Attenuation of Eph Receptor Signaling Is Essential for Spinal Motor Axon Guidance. *Neuron* **2011**, *71* (1), 76–91.

(15) Miao, H.; Li, D. Q.; Mukherjee, A.; Guo, H.; Petty, A.; Cutter, J.; Basilion, J. P.; Sedor, J.; Wu, J.; Danielpour, D.; Sloan, A. E.; Cohen, M. L.; Wang, B. EphA2 Mediates Ligand-Dependent Inhibition and Ligand-Independent Promotion of Cell Migration and Invasion via a Reciprocal Regulatory Loop with Akt. *Cancer Cell* **2009**, *16* (1), 9–20.

(16) Noren, N. K.; Yang, N. Y.; Silldorf, M.; Mutyala, R.; Pasquale, E. B. Ephrin-Independent Regulation of Cell Substrate Adhesion by the EphB4 Receptor. *Biochem. J.* **2009**, *422* (3), 433–442.

(17) Matsuoka, H.; Obama, H.; Kelly, M. L.; Matsui, T.; Nakamoto, M. Biphasic Functions of the Kinase-Defective Ephb6 Receptor in Cell Adhesion and Migration. *J. Biol. Chem.* **2005**, *280* (32), 29355–29363.

(18) Stein, E.; Lane, A. A.; Cerretti, D. P.; Schoecklmann, H. O.; Schroff, A. D.; Van Etten, R. L.; Daniel, T. O. Eph Receptors Discriminate Specific Ligand Oligomers to Determine Alternative Signaling Complexes, Attachment, and Assembly Responses. *Genes Dev.* **1998**, *12* (5), 667–678.

(19) Davis, S.; Gale, N. W.; Aldrich, T. H.; Maisonpierre, P. C.; Lhotak, V.; Pawson, T.; Goldfarb, M.; Yancopoulos, G. D. Ligands for EPH-Related Receptor Tyrosine Kinases That Require Membrane Attachment or Clustering for Activity. *Science* **1994**, *266* (5186), 816–819.

(20) Wimmer-Kleikamp, S. H.; Janes, P. W.; Squire, A.; Bastiaens, P. I. H.; Lakmann, M. Recruitment of Eph Receptors into Signaling Clusters Does Not Require Ephrin Contact. *J. Cell Biol.* **2004**, *164* (5), 661–666.

(21) Miao, H.; Burnett, E.; Kinch, M.; Simon, E.; Wang, B. Activation of EphA2 Kinase Suppresses Integrin Function and Causes Focal-Adhesion-Kinase Dephosphorylation. *Nat. Cell Biol.* **2000**, *2* (2), 62–69.

(22) Singh, D. R.; Kanvinde, P.; King, C.; Pasquale, E. B.; Hristova, K. The EphA2 Receptor Is Activated through Induction of Distinct, Ligand-Dependent Oligomeric Structures. *Commun. Biol.* **2018**, *1* (1), 1–12.

(23) Alford, S. C.; Bazowski, J.; Lorimer, H.; Elowe, S.; Howard, P. L. Tissue Transglutaminase Clusters Soluble A-Type Ephrins into Functionally Active High Molecular Weight Oligomers. *Exp. Cell Res.* **2007**, *313* (20), 4170–4179.

(24) Wykosky, J.; Palma, E.; Gibo, D. M.; Ringler, S.; Turner, C. P.; Debinski, W. Soluble Monomeric EphrinA1 Is Released from Tumor Cells and Is a Functional Ligand for the EphA2 Receptor. *Oncogene* **2008**, *27* (58), 7260–7273.

(25) Himanen, J. P.; Rajashankar, K. R.; Lackmann, M.; Cowan, C. A.; Henkemeyer, M.; Nikolov, D. B. Crystal Structure of an Eph Receptor-Ephrin Complex. *Nature* **2001**, *414* (6866), 933–938.

(26) Chrencik, J. E.; Brooun, A.; Kraus, M. L.; Recht, M. I.; Kolatkar, A. R.; Gye, W. H.; Seifert, J. M.; Widmer, H.; Auer, M.; Kuhn, P. Structural and Biophysical Characterization of the EphB4·EphrinB2 Protein-Protein Interaction and Receptor Specificity. *J. Biol. Chem.* **2006**, *281* (38), 28185–28192.

(27) Himanen, J. P.; Goldgur, Y.; Miao, H.; Myshkin, E.; Guo, H.; Buck, M.; Nguyen, M.; Rajashankar, K. R.; Wang, B.; Nikolov, D. B. Ligand Recognition by A-Class Eph Receptors: Crystal Structures of the EphA2 Ligand-Binding Domain and the EphA2/Ephrin-A1 Complex. *EMBO Rep.* **2009**, *10* (7), 722–728.

(28) Himanen, J. P.; Yermekbayeva, L.; Janes, P. W.; Walker, J. R.; Xu, K.; Atapattu, L.; Rajashankar, K. R.; Mensinga, A.; Lackmann, M.; Nikolov, D. B.; Dhe-Paganon, S. Architecture of Eph Receptor Clusters. *Proc. Natl. Acad. Sci. U. S. A.* **2010**, *107* (24), 10860–10865.

(29) Seiradake, E.; Harlos, K.; Sutton, G.; Aricescu, A. R.; Jones, E. Y. An Extracellular Steric Seeding Mechanism for Eph-Ephrin Signaling Platform Assembly. *Nat. Struct. Mol. Biol.* **2010**, *17* (4), 398–402.

(30) Seiradake, E.; Schaupp, A.; Del Toro Ruiz, D.; Kaufmann, R.; Mitakidis, N.; Harlos, K.; Aricescu, A. R.; Klein, R.; Jones, E. Y. Structurally Encoded Intraclass Differences in EphA Clusters Drive Distinct Cell Responses. *Nat. Struct. Mol. Biol.* **2013**, *20* (8), 958–964.

(31) Singh, D. R.; Ahmed, F.; King, C.; Gupta, N.; Salotto, M.; Pasquale, E. B.; Hristova, K. EphA2 Receptor Unliganded Dimers Suppress EphA2 Pro-Tumorigenic Signaling. *J. Biol. Chem.* **2015**, *290* (45), 27271–27279.

(32) Pitulescu, M. E.; Adams, R. H. Eph/Ephrin Molecules - A Hub for Signaling and Endocytosis. *Genes Dev.* **2010**, *24* (22), 2480–2492.

(33) Janes, P. W.; Saha, N.; Barton, W. A.; Kolev, M. V.; Wimmer-Kleikamp, S. H.; Nievergall, E.; Blobel, C. P.; Himanen, J. P.; Lackmann, M.; Nikolov, D. B. Adam Meets Eph: An ADAM Substrate Recognition Module Acts as a Molecular Switch for Ephrin Cleavage in Trans. *Cell* **2005**, *123* (2), 291–304.

(34) Schaupp, A.; Sabet, O.; Dudanova, I.; Ponserre, M.; Bastiaens, P.; Klein, R. The

Composition of EphB2 Clusters Determines the Strength in the Cellular Repulsion Response. *J. Cell Biol.* **2014**, *204* (3), 409–422.

(35) Salaita, K.; Nair, P. M.; Petit, R. S.; Neve, R. M.; Das, D.; Gray, J. W.; Groves, J. T. Restriction of Receptor Movement Alters Cellular Response: Physical Force Sensing by EphA2. *Science* **2010**, *327* (5971), 1380–1385.

(36) Greene, A. C.; Lord, S. J.; Tian, A.; Rhodes, C.; Kai, H.; Groves, J. T. Spatial Organization of EphA2 at the Cell-Cell Interface Modulates Trans-Endocytosis of EphrinA1. *Biophys. J.* **2014**, *106* (10), 2196–2205.

(37) Dong, M.; Spelke, D. P.; Lee, Y. K.; Chung, J. K.; Yu, C. H.; Schaffer, D. V.; Groves, J. T. Spatiomechanical Modulation of EphB4-Ephrin-B2 Signaling in Neural Stem Cell Differentiation. *Biophys. J.* **2018**, *115* (5), 865–873.

(38) Conway, A.; Vazin, T.; Spelke, D. P.; Rode, N. A.; Healy, K. E.; Kane, R. S.; Schaffer, D. V. Multivalent Ligands Control Stem Cell Behaviour in Vitro and in Vivo. *Nat. Nanotechnol.* **2013**, *8* (11), 831–838.

(39) Shaw, A.; Lundin, V.; Petrova, E.; Fördos, F.; Benson, E.; Al-Amin, A.; Herland, A.; Blokzijl, A.; Högberg, B.; Teixeira, A. I. Spatial Control of Membrane Receptor Function Using Ligand Nanocalipers. *Nat. Methods* **2014**, *11* (8), 841–846.

(40) Liang, L. Y.; Patel, O.; Janes, P. W.; Murphy, J. M.; Lucet, I. S. Eph Receptor Signalling: From Catalytic to Non-Catalytic Functions. *Oncogene* **2019**, *38* (39), 6567–6584.

(41) Miao, H.; Wei, B. R.; Peehl, D. M.; Li, Q.; Alexandrou, T.; Schelling, J. R.; Rhim, J. S.; Sedor, J. R.; Burnett, E.; Wang, B. Activation of EphA Receptor Tyrosine Kinase Inhibits the Ras/MAPK Pathway. *Nat. Cell Biol.* **2001**, *3* (5), 527–530.

(42) Elowe, S.; Holland, S. J.; Kulkarni, S.; Pawson, T. Downregulation of the Ras–Mitogen-Activated Protein Kinase Pathway by the EphB2 Receptor Tyrosine Kinase Is Required for Ephrin-Induced Neurite Retraction. *Mol. Cell. Biol.* **2001**, *21* (21), 7429–7441.

(43) Wykosky, J.; Debinski, W. The EphA2 Receptor and EphrinA1 Ligand in Solid Tumors: Function and Therapeutic Targeting. *Mol. Cancer Res.* **2008**, *6* (12), 1795–1806.

(44) Zelinski, D. P.; Zantek, N. D.; Stewart, J. C.; Irizarry, A. R.; Kinch, M. S. EphA2 Overexpression Causes Tumorigenesis of Mammary Epithelial Cells. *Cancer Res.* **2001**, *61* (5), 2301–2306.

(45) Brantley-Sieders, D. M.; Zhuang, G.; Hicks, D.; Wei, B. F.; Hwang, Y.; Cates, J. M. M.; Coffman, K.; Jackson, D.; Bruckheimer, E.; Muraoka-Cook, R. S.; Chen, J. The

Receptor Tyrosine Kinase EphA2 Promotes Mammary Adenocarcinoma Tumorigenesis and Metastatic Progression in Mice by Amplifying ErbB2 Signaling. *J. Clin. Invest.* **2008**, *118* (1), 64–78.

(46) Miao, H.; Nickel, C. H.; Cantley, L. G.; Bruggeman, L. A.; Bennardo, L. N.; Wang, B. EphA Kinase Activation Regulates HGF-Induced Epithelial Branching Morphogenesis. *J. Cell Biol.* **2003**, *162* (7), 1281–1292.

(47) Dohn, M.; Jiang, J.; Chen, X. Receptor Tyrosine Kinase EphA2 Is Regulated by P53-Family Proteins and Induces Apoptosis. *Oncogene* **2001**, *20* (45), 6503–6515.

(48) Fox, B. P.; Kandpal, R. P. Invasiveness of Breast Carcinoma Cells and Transcript Profile: Eph Receptors and Ephrin Ligands as Molecular Markers of Potential Diagnostic and Prognostic Application. *Biochem. Biophys. Res. Commun.* **2004**, *318* (4), 882–892.

(49) Wykosky, J.; Gibo, D. M.; Stanton, C.; Debinski, W. EphA2 as a Novel Molecular Marker and Target in Glioblastoma Multiforme. *Mol. Cancer Res.* **2005**, *3* (10), 541–551.

(50) Macrae, M.; Neve, R. M.; Rodriguez-Viciana, P.; Haqq, C.; Yeh, J.; Chen, C.; Gray, J. W.; McCormick, F. A Conditional Feedback Loop Regulates Ras Activity through EphA2. *Cancer Cell* **2005**, *8* (2), 111–118.

(51) Hollestelle, A.; Nagel, J. H. A.; Smid, M.; Lam, S.; Elstrodt, F.; Wasielewski, M.; Ng, S. S.; French, P. J.; Peeters, J. K.; Rozendaal, M. J.; Riaz, M.; Koopman, D. G.; Ten Hagen, T. L. M.; De Leeuw, B. H. C. G. M.; Zwarthoff, E. C.; Teunisse, A.; Van Der Spek, P. J.; Klijn, J. G. M.; Dinjens, W. N. M.; Ethier, S. P.; Clevers, H.; Jochemsen, A. G.; Den Bakker, M. A.; Foekens, J. A.; Martens, J. W. M.; Schutte, M. Distinct Gene Mutation Profiles among Luminal-Type and Basal-Type Breast Cancer Cell Lines. *Breast Cancer Res. Treat.* **2010**, *121* (1), 53–64.

(52) Miao, H.; Gale, N. W.; Guo, H.; Qian, J.; Petty, A.; Kaspar, J.; Murphy, A. J.; Valenzuela, D. M.; Yancopoulos, G.; Hambardzumyan, D.; Lathia, J. D.; Rich, J. N.; Lee, J.; Wang, B. EphA2 Promotes Infiltrative Invasion of Glioma Stem Cells in Vivo through Cross-Talk with Akt and Regulates Stem Cell Properties. *Oncogene* **2015**, *34* (5), 558–567.

(53) Barquilla, A.; Lamberto, I.; Noberini, R.; Heynen-Genel, S.; Brill, L. M.; Pasquale, E. B. Protein Kinase A Can Block EphA2 Receptor-Mediated Cell Repulsion by Increasing EphA2 S897 Phosphorylation. *Mol. Biol. Cell* **2016**, *27* (17), 2757–2770.

(54) Zhou, Y.; Yamada, N.; Tanaka, T.; Hori, T.; Yokoyama, S.; Hayakawa, Y.; Yano, S.; Fukuoka, J.; Koizumi, K.; Saiki, I.; Sakurai, H. Crucial Roles of RSK in Cell Motility by Catalysing Serine Phosphorylation of EphA2. *Nat. Commun.* **2015**, *6*, 7679.

(55) Garcia, K. C.; Degano, M.; Stanfield, R. L.; Brunmark, A.; Jackson, M. R.; Peterson, P. A.; Teyton, L.; Wilson, I. A. An Aβ T Cell Receptor Structure at 2.5 Å and Its Orientation in the TCR-MHC Complex. *J. Immunol.* **2010**, *185* (11), 209–219.

(56) Call, M. E.; Pyrdol, J.; Wiedmann, M.; Wucherpfennig, K. W. The Organizing Principle in the Formation of the T Cell Receptor-CD3 Complex. *Cell* **2002**, *111* (7), 967–979.

(57) Van Der Merwe, P. A.; Dushek, O. Mechanisms for T Cell Receptor Triggering. *Nat. Rev. Immunol.* **2011**, *11* (1), 47–55.

(58) Weiss, A.; Littman, D. R. Signal Transduction by Lymphocyte Antigen Receptors. *Cell* **1994**, *76* (2), 263–274.

(59) Dustin, M. L.; Chan, A. C. Signaling Takes Shape in the Immune System. *Cell* **2000**, *103* (2), 283–294.

(60) Fathman, C. G.; Lineberry, N. B. Molecular Mechanisms of CD4+ T-Cell Anergy. *Nat. Rev. Immunol.* **2007**, *7* (8), 599–609.

(61) Norcross, M. A. A Synaptic Basis for T-Lymphocyte Activation. *Ann. l'Institut Pasteur - Immunol.* **1984**, *135* (2), 113–134.

(62) Paul, W. E.; Seder, R. A. Lymphocyte Responses and Cytokines. *Cell* **1994**, *76* (2), 241–251.

(63) Monks, C. R. F.; Freiberg, B. A.; Kupfer, H.; Sciaky, N.; Kupfer, A. Three-Dimensional Segregation of Supramolecular Activation Clusters in T Cells. *Nature* **1998**, *395* (6697), 82–86.

(64) Dustin, M. L.; Olszowy, M. W.; Holdorf, A. D.; Li, J.; Bromley, S.; Desai, N.; Widder, P.; Rosenberger, F.; Van Der Merwe, P. A.; Allen, P. M.; Shaw, A. S. A Novel Adaptor Protein Orchestrates Receptor Patterning and Cytoskeletal Polarity in T-Cell Contacts. *Cell* **1998**, *94* (5), 667–677.

(65) Freiberg, B. A.; Kupfer, H.; Maslanik, W.; Delli, J.; Kappler, J.; Zaller, D. M.; Kupfer, A. Staging and Resetting T Cell Activation in SMACs. *Nat. Immunol.* **2002**, *3* (10), 911–917.

(66) Brossard, C.; Feuillet, V.; Schmitt, A.; Randriamampita, C.; Romao, M.; Raposo, G.; Trautmann, A. Multifocal Structure of the T Cell - Dendritic Cell Synapse. *Eur. J. Immunol.* **2005**, *35* (6), 1741–1753.

(67) Tseng, S.-Y.; Waite, J. C.; Liu, M.; Vardhana, S.; Dustin, M. L. T Cell-Dendritic Cell

Immunological Synapses Contain TCR-Dependent CD28-CD80 Clusters That Recruit Protein Kinase Cθ. *J. Immunol.* **2008**, *181* (7), 4852–4863.

(68) Yu, Y.; Smoligovets, A. A.; Groves, J. T. Modulation of T Cell Signaling by the Actin Cytoskeleton. *J. Cell Sci.* **2013**, *126* (5), 1049–1058.

(69) Grakoui, A.; Bromley, S. K.; Sumen, C.; Davis, M. M.; Shaw, A. S.; Allen, P. M.; Dustin, M. L. The Immunological Synapse: A Molecular Machine Controlling T Cell Activation. *Science* **1999**, *285* (5425), 221–227.

(70) Yokosuka, T.; Sakata-Sogawa, K.; Kobayashi, W.; Hiroshima, M.; Hashimoto-Tane, A.; Tokunaga, M.; Dustin, M. L.; Saito, T. Newly Generated T Cell Receptor Microclusters Initiate and Sustain T Cell Activation by Recruitment of Zap70 and SLP-76. *Nat. Immunol.* **2005**, *6* (12), 1253–1262.

(71) Campi, G.; Varma, R.; Dustin, M. L. Actin and Agonist MHC-Peptide Complex-Dependent T Cell Receptor Microclusters as Scaffolds for Signaling. *J. Exp. Med.* **2005**, *202* (8), 1031–1036.

(72) Yokosuka, T.; Kobayashi, W.; Sakata-Sogawa, K.; Takamatsu, M.; Hashimoto-Tane, A.; Dustin, M. L.; Tokunaga, M.; Saito, T. Spatiotemporal Regulation of T Cell Costimulation by TCR-CD28 Microclusters and Protein Kinase C θ Translocation. *Immunity* **2008**, *29* (4), 589–601.

(73) Kaizuka, Y.; Douglass, A. D.; Varma, R.; Dustin, M. L.; Vale, R. D. Mechanisms for Segregating T Cell Receptor and Adhesion Molecules during Immunological Synapse Formation in Jurkat T Cells. *Proc. Natl. Acad. Sci. U. S. A.* **2007**, *104* (51), 20296–20301.

(74) Varma, R.; Campi, G.; Yokosuka, T.; Saito, T.; Dustin, M. L. T Cell Receptor-Proximal Signals Are Sustained in Peripheral Microclusters and Terminated in the Central Supramolecular Activation Cluster. *Immunity* **2006**, *25* (1), 117–127.

(75) Lee, K. H.; Dinner, A. R.; Tu, C.; Campi, G.; Raychaudhuri, S.; Varma, R.; Sims, T. N.; Burack, W. R.; Wu, H.; Wang, J.; Kanagawa, O.; Markiewicz, M.; Allen, P. M.; Dustin, M. L.; Chakraborty, A. K.; Shaw, A. S. The Immunological Synapse Balances T Cell Receptor Signaling and Degradation. *Science* **2003**, *302* (5648), 1218–1222.

(76) Vardhana, S.; Choudhuri, K.; Varma, R.; Dustin, M. L. Essential Role of Ubiquitin and TSG101 Protein in Formation and Function of the Central Supramolecular Activation Cluster. *Immunity* **2010**, *32* (4), 531–540.

(77) Mossman, K. D.; Campi, G.; Groves, J. T.; Dustin, M. L. Altered TCR Signaling from Geometrically Repatterned Immunological Synapses. *Science* **2005**, *310* (5751), 1191–1193.

(78) Choudhuri, K.; Llodrá, J.; Roth, E. W.; Tsai, J.; Gordo, S.; Wucherpfennig, K. W.; Kam, L. C.; Stokes, D. L.; Dustin, M. L. Polarized Release of T-Cell-Receptor-Enriched Microvesicles at the Immunological Synapse. *Nature* **2014**, *507* (7490), 118–123.

(79) Čemerski, S.; Das, J.; Giurisato, E.; Markiewicz, M. A.; Allen, P. M.; Chakraborty, A. K.; Shaw, A. S. The Balance between T Cell Receptor Signaling and Degradation at the Center of the Immunological Synapse Is Determined by Antigen Quality. *Immunity* **2008**, *29* (3), 414–422.

(80) Lillemeier, B. F.; Mörtelmaier, M. A.; Forstner, M. B.; Huppa, J. B.; Groves, J. T.; Davis, M. M. TCR and Lat Are Expressed on Separate Protein Islands on T Cell Membranes and Concatenate during Activation. *Nat. Immunol.* **2010**, *11* (1), 90–96.

(81) Pageon, S. V.; Tabarin, T.; Yamamoto, Y.; Ma, Y.; Bridgeman, J. S.; Cohnen, A.; Benzing, C.; Gao, Y.; Crowther, M. D.; Tungatt, K.; Dolton, G.; Sewell, A. K.; Price, D. A.; Acuto, O.; Parton, R. G.; Gooding, J. J.; Rossy, J.; Rossjohn, J.; Gaus, K. Functional Role of T-Cell Receptor Nanoclusters in Signal Initiation and Antigen Discrimination. *Proc. Natl. Acad. Sci. U. S. A.* **2016**, *113* (37), E5454–E5463.

(82) Hu, Y. S.; Cang, H.; Lillemeier, B. F. Superresolution Imaging Reveals Nanometer- and Micrometer-Scale Spatial Distributions of T-Cell Receptors in Lymph Nodes. *Proc. Natl. Acad. Sci. U. S. A.* **2016**, *113* (26), 7201–7206.

(83) Rossboth, B.; Arnold, A. M.; Ta, H.; Platzer, R.; Kellner, F.; Huppa, J. B.; Brameshuber, M.; Baumgart, F.; Schütz, G. J. TCRs Are Randomly Distributed on the Plasma Membrane of Resting Antigen-Experienced T Cells. *Nat. Immunol.* **2018**, *19* (8), 821–827.

(84) Brameshuber, M.; Kellner, F.; Rossboth, B. K.; Ta, H.; Alge, K.; Sevcsik, E.; Göhring, J.; Axmann, M.; Baumgart, F.; Gascoigne, N. R. J.; Davis, S. J.; Stockinger, H.; Schütz, G. J.; Huppa, J. B. Monomeric TCRs Drive T Cell Antigen Recognition Article. *Nat. Immunol.* **2018**, *19* (5), 487–496.

(85) Dixon, J. F. P.; Law, J. L.; Favero, J. J. Activation of Human T Lymphocytes by Crosslinking of Anti-CD3 Monoclonal Antibodies. *J. Leukoc. Biol.* **1989**, *46* (3), 214–220.

(86) Minguet, S.; Swamy, M.; Alarcón, B.; Luescher, I. F.; Schamel, W. W. A. Full Activation of the T Cell Receptor Requires Both Clustering and Conformational Changes at CD3. *Immunity* **2007**, *26* (1), 43–54.

(87) Wooldridge, L.; Lissina, A.; Cole, D. K.; Van Den Berg, H. A.; Price, D. A.; Sewell, A. K. Tricks with Tetramers: How to Get the Most from Multimeric Peptide-MHC. *Immunology* **2009**, *126* (2), 147–164.

(88) Ma, Z.; Sharp, K. A.; Janmey, P. A.; Finkel, T. H. Surface-Anchored Monomeric Agonist PMHCs Alone Trigger TCR with High Sensitivity. *PLoS Biol.* **2008**, *6* (2), 0328–0342.

(89) Huang, J.; Brameshuber, M.; Zeng, X.; Xie, J.; Li, Q. jing; Chien, Y. hsiu; Valitutti, S.; Davis, M. M. A Single Peptide-Major Histocompatibility Complex Ligand Triggers Digital Cytokine Secretion in CD4+ T Cells. *Immunity* **2013**, *39* (5), 846–857.

(90) Cochran, J. R.; Cameron, T. O.; Stern, L. J. The Relationship of MHC-Peptide Binding and T Cell Activation Probed Using Chemically Defined MHC Class II Oligomers. *Immunity* **2000**, *12* (3), 241–250.

(91) Krogsgaard, M.; Li, Q. J.; Sumen, C.; Huppa, J. B.; Huse, M.; Davis, M. M. Agonist/Endogenous Peptide-MHC Heterodimers Drive T Cell Activation and Sensitivity. *Nature* **2005**, *434* (7030), 238–243.

(92) Dong, H.; Zhu, G.; Tamada, K.; Chen, L. B7-H1, a Third Member of the B7 Family, Co-Stimulates T-Cell Proliferation and Interleukin-10 Secretion. *Nat. Med.* **1999**, *5* (12), 1365–1369.

(93) Freeman, G. J.; Long, A. J.; Iwai, Y.; Bourque, K.; Chernova, T.; Nishimura, H.; Fitz, L. J.; Malenkovich, N.; Okazaki, T.; Byrne, M. C.; Horton, H. F.; Fouser, L.; Carter, L.; Ling, V.; Bowman, M. R.; Carreno, B. M.; Collins, M.; Wood, C. R.; Honjo, T. Engagement of the PD-1 Immunoinhibitory Receptor by a Novel B7 Family Member Leads to Negative Regulation of Lymphocyte Activation. *J. Exp. Med.* **2000**, *192* (7), 1027–1034.

(94) Latchman, Y.; Wood, C. R.; Chernova, T.; Chaudhary, D.; Borde, M.; Chernova, I.; Iwai, Y.; Long, A. J.; Brown, J. A.; Nunes, R.; Greenfield, E. A.; Bourque, K.; Boussiotis, V. A.; Carter, L. L.; Carreno, B. M.; Malenkovich, N.; Nishimura, H.; Okazaki, T.; Honjo, T.; Sharpe, A. H.; Freeman, G. J. PD-L2 Is a Second Ligand for PD-1 and Inhibits T Cell Activation. *Nat. Immunol.* **2001**, *2* (3), 261–268.

(95) Tseng, S. Y.; Otsuji, M.; Gorski, K.; Huang, X.; Slansky, J. E.; Pai, S. I.; Shalabi, A.; Shin, T.; Pardoll, D. M.; Tsuchiya, H. B7-DC, a New Dendritic Cell Molecule with Potent Costimulatory Properties for T Cells. *J. Exp. Med.* **2001**, *193* (7), 839–845.

(96) Sharpe, A. H.; Pauken, K. E. The Diverse Functions of the PD1 Inhibitory Pathway. *Nat. Rev. Immunol.* **2018**, *18* (3), 153–167.

(97) Nishimura, H.; Nose, M.; Hiai, H.; Minato, N.; Honjo, T. Development of Lupus-like Autoimmune Diseases by Disruption of the PD-1 Gene Encoding an ITIM Motif-Carrying Immunoreceptor. *Immunity* **1999**, *11* (2), 141–151.

(98) Nishimura, H.; Okazaki, T.; Tanaka, Y.; Nakatani, K.; Hara, M.; Matsumori, A.;

Sasayama, S.; Mizoguchi, A.; Hiai, H.; Minato, N.; Honjo, T. Autoimmune Dilated Cardiomyopathy in PD-1 Receptor-Deficient Mice. *Science* **2001**, *291* (5502), 319–322.

(99) Agata, Y.; Kawasaki, A.; Nishimura, H.; Ishida, Y.; Tsubata, T.; Yagita, H.; Honjo, T. Expression of the PD-1 Antigen on the Surface of Stimulated Mouse T and B Lymphocytes. *Int. Immunol.* **1996**, *8* (5), 765–772.

(100) Barber, D. L.; Wherry, E. J.; Masopust, D.; Zhu, B.; Allison, J. P.; Sharpe, A. H.; Freeman, G. J.; Ahmed, R. Restoring Function in Exhausted CD8 T Cells during Chronic Viral Infection. *Nature* **2006**, *439* (7077), 682–687.

(101) Blackburn, S. D.; Shin, H.; Haining, W. N.; Zou, T.; Workman, C. J.; Polley, A.; Betts, M. R.; Freeman, G. J.; Vignali, D. A. A.; Wherry, E. J. Coregulation of CD8+ T Cell Exhaustion by Multiple Inhibitory Receptors during Chronic Viral Infection. *Nat. Immunol.* **2009**, *10* (1), 29–37.

(102) Wherry, E. J.; Kurachi, M. Molecular and Cellular Insights into T Cell Exhaustion. *Nat. Rev. Immunol.* **2015**, *15* (8), 486–499.

(103) Matsuzaki, J.; Gnjatic, S.; Mhawech-Fauceglia, P.; Beck, A.; Miller, A.; Tsuji, T.; Eppolito, C.; Qian, F.; Lele, S.; Shrikant, P.; Old, L. J.; Odunsi, K. Tumor-Infiltrating NY-ESO-1-Specific CD8+ T Cells Are Negatively Regulated by LAG-3 and PD-1 in Human Ovarian Cancer. *Proc. Natl. Acad. Sci. U. S. A.* **2010**, *107* (17), 7875–7880.

(104) Kim, A.; Lee, S. J.; Kim, Y. K.; Park, W. Y.; Park, D. Y.; Kim, J. Y.; Lee, C. H.; Gong, G.; Huh, G. Y.; Choi, K. U. Programmed Death-Ligand 1 (PD-L1) Expression in Tumour Cell and Tumour Infiltrating Lymphocytes of HER2-Positive Breast Cancer and Its Prognostic Value. *Sci. Rep.* **2017**, *7* (1).

(105) Ahmadzadeh, M.; Johnson, L. A.; Heemskerk, B.; Wunderlich, J. R.; Dudley, M. E.; White, D. E.; Rosenberg, S. A. Tumor Antigen-Specific CD8 T Cells Infiltrating the Tumor Express High Levels of PD-1 and Are Functionally Impaired. *Blood* **2009**, *114* (8), 1537–1544.

(106) Hirano, F.; Kaneko, K.; Tamura, H.; Dong, H.; Wang, S.; Ichikawa, M.; Rietz, C.; Flies, D. B.; Lau, J. S.; Zhu, G.; Tamada, K.; Chen, L. Blockade of B7-H1 and PD-1 by Monoclonal Antibodies Potentiates Cancer Therapeutic Immunity. *Cancer Res.* **2005**, *65* (3), 1089–1096.

(107) Iwai, Y.; Ishida, M.; Tanaka, Y.; Okazaki, T.; Honjo, T.; Minato, N. Involvement of PD-L1 on Tumor Cells in the Escape from Host Immune System and Tumor Immunotherapy by PD-L1 Blockade. *Proc. Natl. Acad. Sci. U. S. A.* **2002**, *99* (19), 12293–12297.

(108) Wei, S. C.; Duffy, C. R.; Allison, J. P. Fundamental Mechanisms of Immune Checkpoint

Blockade Therapy. *Cancer Discov.* **2018**, *8* (9), 1069–1086.

(109) Pentcheva-Hoang, T.; Chen, L.; Pardoll, D. M.; Allison, J. P. Programmed Death-1 Concentration at the Immunological Synapse Is Determined by Ligand Affinity and Availability. *Proc. Natl. Acad. Sci. U. S. A.* **2007**, *104* (45), 17765–17770.

(110) Yokosuka, T.; Takamatsu, M.; Kobayashi-Imanishi, W.; Hashimoto-Tane, A.; Azuma, M.; Saito, T. Programmed Cell Death 1 Forms Negative Costimulatory Microclusters That Directly Inhibit T Cell Receptor Signaling by Recruiting Phosphatase SHP2. *J. Exp. Med.* **2012**, *209* (6), 1201–1217.

(111) Hui, E.; Cheung, J.; Zhu, J.; Su, X.; Taylor, M. J.; Wallweber, H. A.; Sasmal, D. K.; Huang, J.; Kim, J. M.; Mellman, I.; Vale, R. D. T Cell Costimulatory Receptor CD28 Is a Primary Target for PD-1-Mediated Inhibition. *Science* **2017**, *355* (6332), 1428–1433.

(112) Zhao, Y.; Harrison, D. L.; Song, Y.; Ji, J.; Huang, J.; Hui, E. Antigen-Presenting Cell-Intrinsic PD-1 Neutralizes PD-L1 in Cis to Attenuate PD-1 Signaling in T Cells. *Cell Rep.* **2018**, *24* (2), 379-390.e6.

(113) Sheppard, K. A.; Fitz, L. J.; Lee, J. M.; Benander, C.; George, J. A.; Wooters, J.; Qiu, Y.; Jussif, J. M.; Carter, L. L.; Wood, C. R.; Chaudhary, D. PD-1 Inhibits T-Cell Receptor Induced Phosphorylation of the ZAP70/CD3ζ Signalosome and Downstream Signaling to PKCθ. *FEBS Lett.* **2004**, *574* (1–3), 37–41.

(114) Patsoukis, N.; Duke-Cohan, J. S.; Chaudhri, A.; Aksoylar, H. I.; Wang, Q.; Council, A.; Berg, A.; Freeman, G. J.; Boussiotis, V. A. Interaction of SHP-2 SH2 Domains with PD-1 ITSM Induces PD-1 Dimerization and SHP-2 Activation. *Commun. Biol.* **2020**, *3* (1).

(115) Celis-Gutierrez, J.; Blattmann, P.; Zhai, Y.; Jarmuzynski, N.; Ruminski, K.; Grégoire, C.; Ounoughene, Y.; Fiore, F.; Aebersold, R.; Roncagalli, R.; Gstaiger, M.; Malissen, B. Quantitative Interactomics in Primary T Cells Provides a Rationale for Concomitant PD-1 and BTLA Coinhibitor Blockade in Cancer Immunotherapy. *Cell Rep.* **2019**, *27* (11), 3315-3330.e7.

(116) Xu, X.; Hou, B.; Fulzele, A.; Masubuchi, T.; Zhao, Y.; Wu, Z.; Hu, Y.; Jiang, Y.; Ma, Y.; Wang, H.; Bennett, E. J.; Fu, G.; Hui, E. PD-1 and BTLA Regulate T Cell Signaling Differentially and Only Partially through SHP1 and SHP2. *J. Cell Biol.* **2020**, *219* (6).

(117) Rota, G.; Niogret, C.; Dang, A. T.; Barros, C. R.; Fonta, N. P.; Alfei, F.; Morgado, L.; Zehn, D.; Birchmeier, W.; Vivier, E.; Guarda, G. Shp-2 Is Dispensable for Establishing T Cell Exhaustion and for PD-1 Signaling in Vivo. *Cell Rep.* **2018**, *23* (1), 39–49.

(118) Mizuno, R.; Sugiura, D.; Shimizu, K.; Maruhashi, T.; Watada, M.; Okazaki, I. mi; Okazaki, T. PD-1 Primarily Targets TCR Signal in the Inhibition of Functional T Cell

Activation. *Front. Immunol.* **2019**, *10* (630).

(119) Kamphorst, A. O.; Wieland, A.; Nasti, T.; Yang, S.; Zhang, R.; Barber, D. L.; Konieczny, B. T.; Daugherty, C. Z.; Koenig, L.; Yu, K.; Sica, G. L.; Sharpe, A. H.; Freeman, G. J.; Blazar, B. R.; Turka, L. A.; Owonikoko, T. K.; Pillai, R. N.; Ramalingam, S. S.; Araki, K.; Ahmed, R. Rescue of Exhausted CD8 T Cells by PD-1-Targeted Therapies Is CD28-Dependent. *Science* **2017**, *355* (6332), 1423–1427.

(120) Demetriou, P.; Abu-Shah, E.; Valvo, S.; McCuaig, S.; Mayya, V.; Kvalvaag, A.; Starkey, T.; Korobchevskaya, K.; Lee, L. Y. W.; Friedrich, M.; Mann, E.; Kutuzov, M. A.; Morotti, M.; Wietek, N.; Rada, H.; Yusuf, S.; Afrose, J.; Siokis, A.; Allan, P.; Ambrose, T.; Arancibia, C.; Bailey, A.; Barnes, E.; Bird-Lieberman, E.; Bornschein, J.; Brain, O.; Braden, B.; Collier, J.; Cobbold, J.; Culver, E.; East, J.; Howarth, L.; Klenerman, P.; Leedham, S.; Palmer, R.; Pavlides, M.; Powrie, F.; Rodrigues, A.; Satsangi, J.; Simmons, A.; Sullivan, P.; Uhlig, H.; Walsh, A.; Meyer-Hermann, M.; Ahmed, A. A.; Depoil, D.; Dustin, M. L. A Dynamic CD2-Rich Compartment at the Outer Edge of the Immunological Synapse Boosts and Integrates Signals. *Nat. Immunol.* **2020**, *21* (10), 1232–1243.

(121) Zhang, X.; Schwartz, J. C. D.; Guo, X.; Bhatia, S.; Cao, E.; Chen, L.; Zhang, Z. Y.; Edidin, M. A.; Nathenson, S. G.; Almo, S. C. Structural and Functional Analysis of the Costimulatory Receptor Programmed Death-1. *Immunity* **2004**, *20* (3), 337–347.

(122) Zak, K. M.; Kitel, R.; Przetocka, S.; Golik, P.; Guzik, K.; Musielak, B.; Dömling, A.; Dubin, G.; Holak, T. A. Structure of the Complex of Human Programmed Death 1, PD-1, and Its Ligand PD-L1. *Structure* **2015**, *23* (12), 2341–2348.

(123) Zak, K. M.; Grudnik, P.; Guzik, K.; Zieba, B. J.; Musielak, B.; Dömling, A.; Dubin, G.; Holak, T. A. Structural Basis for Small Molecule Targeting of the Programmed Death Ligand 1 (PD-L1). *Oncotarget* **2016**, *7* (21), 30323–30335. https://doi.org/10.18632/oncotarget.8730.

(124) Skalniak, L.; Zak, K. M.; Guzik, K.; Magiera, K.; Musielak, B.; Pachota, M.; Szelazek, B.; Kocik, J.; Grudnik, P.; Tomala, M.; Krzanik, S.; Pyrc, K.; Dömling, A.; Dubin, G.; Holak, T. A. Small-Molecule Inhibitors of PD-1/PD-L1 Immune Checkpoint Alleviate the PD-L1-Induced Exhaustion of T-Cells. *Oncotarget* **2017**, *8* (42), 72167–72181.

(125) Mahoney, K. M.; Shukla, S. A.; Patsoukis, N.; Chaudhri, A.; Browne, E. P.; Arazi, A.; Eisenhaure, T. M.; Pendergraft, W. F.; Hua, P.; Pham, H. C.; Bu, X.; Zhu, B.; Hacohen, N.; Fritsch, E. F.; Boussiotis, V. A.; Wu, C. J.; Freeman, G. J. A Secreted PD-L1 Splice Variant That Covalently Dimerizes and Mediates Immunosuppression. *Cancer Immunol. Immunother.* **2019**, *68* (3), 421–432.

(126) Rothemund, P. W. K. Folding DNA to Create Nanoscale Shapes and Patterns. *Nature* **2006**, *440* (7082), 297–302.

(127) Andersen, E. S.; Dong, M.; Nielsen, M. M.; Jahn, K.; Subramani, R.; Mamdouh, W.; Golas, M. M.; Sander, B.; Stark, H.; Oliveira, C. L. P.; Pedersen, J. S.; Birkedal, V.; Besenbacher, F.; Gothelf, K. V.; Kjems, J. Self-Assembly of a Nanoscale DNA Box with a Controllable Lid. *Nature* **2009**, *459* (7243), 73–76.

(128) Douglas, S. M.; Dietz, H.; Liedl, T.; Högberg, B.; Graf, F.; Shih, W. M. Self-Assembly of DNA into Nanoscale Three-Dimensional Shapes. *Nature* **2009**, *459* (7245), 414–418.

(129) Dietz, H.; Douglas, S. M.; Shih, W. M. Folding DNA into Twisted and Curved Nanoscale Shapes. *Science* **2009**, *325* (5941), 725–730.

(130) Han, D.; Pal, S.; Nangreave, J.; Deng, Z.; Liu, Y.; Yan, H. DNA Origami with Complex Curvatures in Three-Dimensional Space. *Science* **2011**, *332* (6027), 342–346.

(131) Castro, C. E.; Kilchherr, F.; Kim, D. N.; Shiao, E. L.; Wauer, T.; Wortmann, P.; Bathe, M.; Dietz, H. A Primer to Scaffolded DNA Origami. *Nat. Methods* **2011**, *8* (3), 221–229.

(132) Ke, Y.; Douglas, S. M.; Liu, M.; Sharma, J.; Cheng, A.; Leung, A.; Liu, Y.; Shih, W. M.; Yan, H. Multilayer DNA Origami Packed on a Square Lattice. *J. Am. Chem. Soc.* **2009**, *131* (43), 15903–15908.

(133) Douglas, S. M.; Marblestone, A. H.; Teerapittayanon, S.; Vazquez, A.; Church, G. M.; Shih, W. M. Rapid Prototyping of 3D DNA-Origami Shapes with CaDNAno. *Nucleic Acids Res.* **2009**, *37* (15), 5001–5006.

(134) Benson, E.; Mohammed, A.; Gardell, J.; Masich, S.; Czeizler, E.; Orponen, P.; Högberg, B. DNA Rendering of Polyhedral Meshes at the Nanoscale. *Nature* **2015**, *523* (7561), 441–444.

(135) Zhang, F.; Jiang, S.; Wu, S.; Li, Y.; Mao, C.; Liu, Y.; Yan, H. Complex Wireframe DNA Origami Nanostructures with Multi-Arm Junction Vertices. *Nat. Nanotechnol.* **2015**, *10* (9), 779–784.

(136) Veneziano, R.; Ratanalert, S.; Zhang, K.; Zhang, F.; Yan, H.; Chiu, W.; Bathe, M. Designer Nanoscale DNA Assemblies Programmed from the Top Down. *Science* **2016**, *352* (6293).

(137) Benson, E.; Mohammed, A.; Bosco, A.; Teixeira, A. I.; Orponen, P.; Högberg, B. Computer-Aided Production of Scaffolded DNA Nanostructures from Flat Sheet Meshes. *Angew. Chemie - Int. Ed.* **2016**, *55* (31), 8869–8872.

(138) Jun, H.; Zhang, F.; Shepherd, T.; Ratanalert, S.; Qi, X.; Yan, H.; Bathe, M. Autonomously Designed Free-Form 2D DNA Origami. *Sci. Adv.* **2019**, *5* (1).

(139) Drew, H. R.; Wing, R. M.; Takano, T.; Broka, C.; Tanaka, S.; Itakura, K.; Dickerson, R. E. Structure of a B-DNA Dodecamer: Conformation and Dynamics. *Proc. Natl. Acad. Sci. U. S. A.* **1981**, *78* (4), 2179–2183.

(140) Ke, Y.; Lindsay, S.; Chang, Y.; Liu, Y.; Yan, H. Self-Assembled Water-Soluble Nucleic Acid Probe Tiles for Label-Free RNA Hybridization Assays. *Science* **2008**, *319* (5860), 180–183.

(141) Rinker, S.; Ke, Y.; Liu, Y.; Chhabra, R.; Yan, H. Self-Assembled DNA Nanostructures for Distance-Dependent Multivalent Ligand-Protein Binding. *Nat. Nanotechnol.* **2008**, *3* (7), 418–422.

(142) Voigt, N. V.; Tørring, T.; Rotaru, A.; Jacobsen, M. F.; Ravnsbæk, J. B.; Subramani, R.; Mamdouh, W.; Kjems, J.; Mokhir, A.; Besenbacher, F.; Gothelf, K. V. Single-Molecule Chemical Reactions on DNA Origami. *Nat. Nanotechnol.* **2010**, *5* (3), 200–203.

(143) Derr, N. D.; Goodman, B. S.; Jungmann, R.; Leschziner, A. E.; Shih, W. M.; Reck-Peterson, S. L. Tug-of-War in Motor Protein Ensembles Revealed with a Programmable DNA Origami Scaffold. *Science* **2012**, *338* (6107), 662–665.

(144) Hartl, C.; Frank, K.; Amenitsch, H.; Fischer, S.; Liedl, T.; Nickel, B. Position Accuracy of Gold Nanoparticles on DNA Origami Structures Studied with Small-Angle X-Ray Scattering. *Nano Lett.* **2018**, *18* (4), 2609–2615.

(145) Bui, H.; Onodera, C.; Kidwell, C.; Tan, Y.; Graugnard, E.; Kuang, W.; Lee, J.; Knowlton, W. B.; Yurke, B.; Hughes, W. L. Programmable Periodicity of Quantum Dot Arrays with DNA Origami Nanotubes. *Nano Lett.* **2010**, *10* (9), 3367–3372.

(146) Sun, W.; Boulais, E.; Hakobyan, Y.; Wang, W. L.; Guan, A.; Bathe, M.; Yin, P. Casting Inorganic Structures with DNA Molds. *Science* **2014**, *346* (6210).

(147) Liu, W.; Halverson, J.; Tian, Y.; Tkachenko, A. V.; Gang, O. Self-Organized Architectures from Assorted DNA-Framed Nanoparticles. *Nat. Chem.* **2016**, *8* (9), 867–873.

(148) Le, J. V.; Luo, Y.; Darcy, M. A.; Lucas, C. R.; Goodwin, M. F.; Poirier, M. G.; Castro, C. E. Probing Nucleosome Stability with a DNA Origami Nanocaliper. *ACS Nano* **2016**, *10* (7), 7073–7084.

(149) Fu, J.; Yang, Y. R.; Dhakal, S.; Zhao, Z.; Liu, M.; Zhang, T.; Walter, N. G.; Yan, H. Assembly of Multienzyme Complexes on DNA Nanostructures. *Nat. Protoc.* **2016**, *11* (11), 2243–2273.

(150) Shaw, A.; Hoffecker, I. T.; Smyrlaki, I.; Rosa, J.; Grevys, A.; Bratlie, D.; Sandlie, I.;

Michaelsen, T. E.; Andersen, J. T.; Högberg, B. Binding to Nanopatterned Antigens Is Dominated by the Spatial Tolerance of Antibodies. *Nat. Nanotechnol.* **2019**, *14* (2), 184–190.

(151) Steinhauer, C.; Jungmann, R.; Sobey, T. L.; Simmel, F. C.; Tinnefeld, P. DNA Origami as a Nanoscopic Ruler for Superresolution Microscopy. *Angew. Chemie - Int. Ed.* **2009**, *48* (47), 8870–8873.

(152) Schmied, J. J.; Raab, M.; Forthmann, C.; Pibiri, E.; Wünsch, B.; Dammeyer, T.; Tinnefeld, P. DNA Origami-Based Standards for Quantitative Fluorescence Microscopy. *Nat. Protoc.* **2014**, *9* (6), 1367–1391.

(153) Raab, M.; Jusuk, I.; Molle, J.; Buhr, E.; Bodermann, B.; Bergmann, D.; Bosse, H.; Tinnefeld, P. Using DNA Origami Nanorulers as Traceable Distance Measurement Standards and Nanoscopic Benchmark Structures. *Sci. Rep.* **2018**, *8* (1).

(154) Veneziano, R.; Moyer, T. J.; Stone, M. B.; Wamhoff, E. C.; Read, B. J.; Mukherjee, S.; Shepherd, T. R.; Das, J.; Schief, W. R.; Irvine, D. J.; Bathe, M. Role of Nanoscale Antigen Organization on B-Cell Activation Probed Using DNA Origami. *Nat. Nanotechnol.* **2020**, *15* (8), 716–723.

(155) Douglas, S. M.; Bachelet, I.; Church, G. M. A Logic-Gated Nanorobot for Targeted Transport of Molecular Payloads. *Science* **2012**, *335* (6070), 831–834.

(156) Zhao, Y. X.; Shaw, A.; Zeng, X.; Benson, E.; Nyström, A. M.; Högberg, B. DNA Origami Delivery System for Cancer Therapy with Tunable Release Properties. *ACS Nano* **2012**, *6* (10), 8684–8691.

(157) Zhang, Q.; Jiang, Q.; Li, N.; Dai, L.; Liu, Q.; Song, L.; Wang, J.; Li, Y.; Tian, J.; Ding, B.; Du, Y. DNA Origami as an in Vivo Drug Delivery Vehicle for Cancer Therapy. *ACS Nano* **2014**, *8* (7), 6633–6643.

(158) Schüller, V. J.; Heidegger, S.; Sandholzer, N.; Nickels, P. C.; Suhartha, N. A.; Endres, S.; Bourquin, C.; Liedl, T. Cellular Immunostimulation by CpG-Sequence-Coated DNA Origami Structures. *ACS Nano* **2011**, *5* (12), 9696–9702.

(159) Rahman, M. A.; Wang, P.; Zhao, Z.; Wang, D.; Nannapaneni, S.; Zhang, C.; Chen, Z.; Griffith, C. C.; Hurwitz, S. J.; Chen, Z. G.; Ke, Y.; Shin, D. M. Systemic Delivery of Bc12-Targeting SiRNA by DNA Nanoparticles Suppresses Cancer Cell Growth. *Angew. Chemie - Int. Ed.* **2017**, *56* (50), 16023–16027.

(160) Liu, S.; Jiang, Q.; Zhao, X.; Zhao, R.; Wang, Y.; Wang, Y.; Liu, J.; Shang, Y.; Zhao, S.; Wu, T.; Zhang, Y.; Nie, G.; Ding, B. A DNA Nanodevice-Based Vaccine for Cancer Immunotherapy. *Nat. Mater.* **2021**, *20*, 421–430.

(161) Cong, Y.; Pawlisz, E.; Bryant, P.; Balan, S.; Laurine, E.; Tommasi, R.; Singh, R.; Dubey, S.; Peciak, K.; Bird, M.; Sivasankar, A.; Swierkosz, J.; Muroni, M.; Heidelberger, S.; Farys, M.; Khayrzad, F.; Edwards, J.; Badescu, G.; Hodgson, I.; Heise, C.; Somavarapu, S.; Liddell, J.; Powell, K.; Zloh, M.; Choi, J. W.; Godwin, A.; Brocchini, S. Site-Specific PEGylation at Histidine Tags. *Bioconjug. Chem.* **2012**, *23* (2), 248–263.

(162) Söderberg, O.; Gullberg, M.; Jarvius, M.; Ridderstråle, K.; Leuchowius, K. J.; Jarvius, J.; Wester, K.; Hydbring, P.; Bahram, F.; Larsson, L. G.; Landegren, U. Direct Observation of Individual Endogenous Protein Complexes in Situ by Proximity Ligation. *Nat. Methods* **2006**, *3* (12), 995–1000.

(163) Chozinski, T. J.; Gagnon, L. A.; Vaughan, J. C. Twinkle, Twinkle Little Star: Photoswitchable Fluorophores for Super-Resolution Imaging. *FEBS Lett.* **2014**, *588* (19), 3603–3612.

(164) Picelli, S.; Faridani, O. R.; Björklund, Å. K.; Winberg, G.; Sagasser, S.; Sandberg, R. Full-Length RNA-Seq from Single Cells Using Smart-Seq2. *Nat. Protoc.* **2014**, *9* (1), 171–181.